

Snapshot compressed sensing: performance bounds and algorithms

Shirin Jalali and Xin Yuan

Abstract

Snapshot compressed sensing (CS) refers to compressive imaging systems where multiple frames are mapped into a single measurement frame. Each pixel in the acquired frame is a linear combination of the corresponding pixels in the frames that are collapsed together. While the problem can be cast as a CS problem, due to the very special structure of the sensing matrix, standard CS theory cannot be employed to study such systems. In this paper, a compression-based framework is proposed that enable a theoretical analysis of snapshot compressive sensing systems. This new framework leads to two novel, computationally-efficient and theoretically-analyzable snapshot compressive sensing recovery algorithms. The proposed algorithms are iterative and employ compression codes to impose structure on the recovered frames. Theoretical convergence guarantees are derived for both algorithms. In simulations, it is shown that combining the proposed algorithms with a customized video compression code designed to exploit nonlocal structures of video frames significantly improves the state-of-the-art performance.

I. INTRODUCTION

There have been significant theoretical advances in compressed sensing (CS) since the seminal works of [2] and [3]. Most of such theoretical results are derived assuming that the sensing matrix is a dense matrix and its entries are independently and identically distributed (i.i.d.) according to some distribution. In the meantime, various *compressive imaging* systems have been built [4]–[9], and convincing results have been obtained in diverse applications, such as video CS [7]–[9] and hyper-spectral image CS [6], [10], [11]. However, except for the single-pixel camera [4] and similar architectures [12], [13], the sensing matrices employed in most of these practical systems are usually not random, and typically *structured* very differently compared to random sensing matrices studied in the CS literature.

One common property of such imaging systems is that in many of them, due to hardware constraints, unlike standard CS, each measurement only depends on few entries of the input signal. For example, in some video CS systems, high-speed frames are modulated at a higher frequency than the capture rate of the camera, which is working at a low frame rate. Moreover, each measured pixel in the captured frame only depends on the pixels

This paper was presented in part at 2018 IEEE International Symposium on Information Theory, Vail, Colorado [1].

The authors are with Nokia Bell Labs, 600 Mountain Avenue, Murray Hill, NJ, 07974, USA, {shirin.jalali, xin_x.yuan}@nokia-bell-labs.com

located at the same position in the input frames. In this manner, each captured measurement frame can recover a number of high-speed frames, depending on the coding strategy, e.g., 148 frames reconstructed from a snapshot in [8]. These systems can be recognized as snapshot compressive imaging systems. Given the special structure of the sensing matrix in such systems, the traditional CS theory¹ does not apply to such applications. Therefore, a new theory is desired for these *snapshot compressed sensing* systems.

A. Motivation

In standard CS, the measurement system is usually modeled as

$$\mathbf{y} = \Phi \mathbf{x} + \mathbf{z}, \quad (1)$$

where $\Phi \in \mathbb{R}^{m \times n}$, $m \ll n$, denotes the sensing matrix, $\mathbf{x} \in \mathbb{R}^n$ is the desired signal and $\mathbf{z} \in \mathbb{R}^m$ denotes the noise. Clearly, recovery of \mathbf{x} from measurements \mathbf{y} is only possible if the input signal is *structured*. For various types of structure such as sparsity, group-sparsity, etc., it is known that efficient algorithms exist to robustly recover \mathbf{x} from measurements \mathbf{y} .

In parallel to advances in CS theory and algorithms, a hyperspectral compressive imaging system called coded aperture snapshot spectral imaging (CASSI) was built in 2007 [6]. CASSI recovers a three-dimensional (3D) spectral data cube, in which more than 30 frequency channels (images) at different wavelengths have been reconstructed, from a single two-dimensional (2D) captured measurement. This coded aperture modulating strategy has paved the way for many high-dimensional compressive imaging systems, from the aforementioned video CS to depth CS [17], [18], polarization CS [19], and joint temporal-spectral CS [20].

The measurement process in such hardware systems can typically be modeled as [8], [11]

$$\mathbf{y} = \mathbf{H} \mathbf{x} + \mathbf{z}, \quad (2)$$

where \mathbf{H} , the sensing matrix, follows a very specific structure and can be written as

$$\mathbf{H} = [\mathbf{D}_1, \dots, \mathbf{D}_B], \quad (3)$$

where $\{\mathbf{D}_k\}_{k=1}^B$ are diagonal matrices. It can be observed that, unlike matrices used in standard CS, here the sensing matrix is very sparse. As an example, consider the video CS system described in [8], where B high-speed frames $\{\mathbf{X}_k\}_{k=1}^B$, $\mathbf{X}_k \in \mathbb{R}^{n_x \times n_y}$, are modulated by masks $\{\mathbf{C}_k\}_{k=1}^B$, $\mathbf{C}_k \in \mathbb{R}^{n_x \times n_y}$. The 2D measurement $\mathbf{Y} \in \mathbb{R}^{n_x \times n_y}$

¹Structured sensing matrices in CS have been studied, e.g., in [14]–[16]. However, the sensing matrices considered therein are different from the one used in snapshot CS and thus are out of the scope of this paper.

is given by

$$\mathbf{Y} = \sum_{k=1}^B \mathbf{X}_k \odot \mathbf{C}_k + \mathbf{Z}. \quad (4)$$

Here all B pixels located at position (i, j) , $(i, j) \in \{1, \dots, n_x\} \times \{1, \dots, n_y\}$, are measured together as

$$y_{i,j} = \sum_{k=1}^B c_{i,j,k} x_{i,j,k} + z_{i,j}. \quad (5)$$

This can also be stated in the vector formulation of (2), by defining

$$\mathbf{x} = [\mathbf{x}_1^\top, \dots, \mathbf{x}_B^\top]^\top, \quad (6)$$

where $\mathbf{x}_k = \text{vec}(\mathbf{X}_k)$, and $\mathbf{D}_k = \text{diag}(\text{vec}(\mathbf{C}_k))$, for $k = 1, \dots, B$. Thus $\mathbf{x} \in \mathbb{R}^{n_x n_y B}$, $\mathbf{H} \in \mathbb{R}^{n_x n_y \times (n_x n_y B)}$. *The sampling rate here is equal to $1/B$.*

While snapshot CS systems have delivered promising results in practice, not much theoretical analysis of such systems have been developed yet. Two major aspects that differentiate theoretical analysis of snapshot CS systems from that of standard CS systems are the following:

- i) In snapshot CS systems, the sensing matrix follows a very special structure and is very sparse. Due to this special structure, it is for instance straightforward to check that such matrices do not satisfy standard conditions, such as RIP or mutual coherence [21] that are used in standard CS.²
- ii) More importantly, it is challenging to develop a mathematical model for multi-frame signals such as videos that captures both their inter-frame and their intra-frame dependencies.

B. Contributions of This Paper

The above research gap³ between the existing theory and real hardware implementations leads to the following fundamental questions about snapshot CS systems:

- 1) Is it *theoretically* possible to recover \mathbf{x} from the measurement \mathbf{y} defined in (2), for $B > 1$?
- 2) What is the maximum number of frames B that can be mapped to a single measurement and still be able to recover the signal \mathbf{x} and how it is related to the structure of the signal \mathbf{x} ?
- 3) Are there efficient and *theoretically-analyzable* recovery algorithms for snapshot CS systems?

In this paper, inspired by the idea of compression-based CS [25], we develop a theoretical framework for snapshot CS. We also propose two efficient iterative snapshot CS algorithms with convergence guarantees. Though various algorithms, *e.g.*, [26]–[28], have been developed for video and hyper-spectral image CS, to our best knowledge, no

²For instance, for a sensing matrix of the form described in (3), *i*) the *spark* [22] of \mathbf{H} is $\text{spark}(\mathbf{H}) = 2$, since for any $j = 1, \dots, n - 1$, \mathbf{h}_j and \mathbf{h}_{j+B} are linearly dependent; recall that the *spark* of a given matrix is the smallest number of columns that are linearly-dependent, and *ii*) the mutual coherence [23] of \mathbf{H} is $\mu(\mathbf{H}) = 1$.

³A tutorial was presented in [24] on CS for practical optical imaging systems. However, it did not fill the research gap described here.

theoretical guarantees have been available yet for the special structure of sensing matrices that arise in snapshot CS.

C. Related work

As mentioned earlier, theoretical work in the CS literature is mainly focused on sparse signals [3], [21] and their extensions such as group-sparsity [29], model-based sparsity [30], and the low-rank property [31]. Many classes of signals such as natural images and videos typically follow much more complex patterns than these structures. A recovery algorithm that takes advantage of those complex structures, potentially, can outperform standard schemes by requiring a lower sampling rate or having a better reconstruction quality. However, designing and analyzing such recovery algorithms that impose both the measurement constraints and the source's known patterns is in general very challenging. One recent approach to address this issue is to take advantage of algorithms that are designed for other data processing tasks such as denoising or data compression and to derive for instance denoising-based [32] or compression-based [25] recovery algorithms. The advantage of this approach is that, without much additional effort, it elevates the scope of structures used by CS recovery algorithms to those used by denoising or compression algorithms. As an example, modern image compression algorithms such as JPEG and JPEG2000 [33] are very efficient codes that are designed to exploit various common properties of natural images. Therefore, a CS recovery algorithm that employs JPEG2000 to impose structure on the recovered signal, ideally is a recovery algorithm that searches for a signal that is consistent with the measurements and at the same time satisfies the image properties used by the JPEG2000 code. This line of work of designing compression-based CS was first started in [25] and then later continued in [34], where the authors proposed an efficient compression-based recovery algorithm that achieves state-of-the-art performance in image CS.

Additionally, there are other CS systems such as those studied in [13], [35] for video CS, and [36] for hyperspectral imaging. (Please refer to the survey in [37]–[39] for more details on such systems.) While the sensing matrices used in these works are different from the one used in snapshot CS, they have some similarities with the sensing matrix defined in (3). We expect that our proposed compression-based framework, with some minor modifications, can be applied in such cases as well and paves the way for performing theoretical analysis of such systems too.

D. Notation and Organization

Matrices are denoted by upper-case bold letters such as \mathbf{X} and \mathbf{Y} . For a matrix $\mathbf{X} \in \mathbb{R}^{n_1 \times n_2}$, let $X_{i,j}$ denote its (i, j) -th element. For matrices $\mathbf{X} \in \mathbb{R}^{n_1 \times n_2}$ and $\mathbf{Y} \in \mathbb{R}^{n_1 \times n_2}$, $\mathbf{Z} = \mathbf{X} \odot \mathbf{Y}$ denote their inner product, where for $(i, j) \in \{1, \dots, n_1\} \times \{1, \dots, n_2\}$, $Z_{ij} = X_{ij}Y_{ij}$. Vectors are denoted by bold lower-case letters, such as \mathbf{x} and \mathbf{y} . For $\mathbf{x} \in \mathbb{R}^n$ and $\mathbf{y} \in \mathbb{R}^n$, $\langle \mathbf{x}, \mathbf{y} \rangle = \sum_{i=1}^n x_i y_i$ denotes their inner product. Sets are denoted by calligraphic letters such as \mathcal{X} and \mathcal{Y} . The size of a set \mathcal{X} is denoted as $|\mathcal{X}|$. Throughout the paper, \log and \ln refer to logarithm in

base 2 and natural logarithm, respectively. Vectors are denoted by bold lower-case letters, such as \mathbf{x} and \mathbf{y} , and matrices are denoted by bold upper-case letters, such as \mathbf{H} .

The rest of this paper is organized as follows. Section II briefly reviews the definitions of lossy compression codes for multi-frame signals and the performance of a compression-based snapshot CS recovery method. Section III introduces two different efficient compression-based recovery methods for snapshot CS in subsections III-A and III-B and proves that they both converge. Simulation results of video CS are shown in Section IV. Section V provides proofs of the main results of the paper and Section VI concludes the paper.

II. DATA COMPRESSION FOR SNAPSHOT CS

Our proposed framework studies snapshot CS systems via utilizing data compression codes. In the following, we first briefly review the definitions of lossy compression codes for multi-frame signals, and then develop our snapshot CS theory based on data compression.

A. Data Compression

Consider a compact set $\mathcal{Q} \subset \mathbb{R}^{nB}$. Each signal $\mathbf{x} \in \mathcal{Q}$, consists of B vectors (frames) $\{\mathbf{x}_1, \dots, \mathbf{x}_B\}$ in \mathbb{R}^n , with $n = n_x n_y$ as shown in (6). A lossy compression code of rate r for \mathcal{Q} is characterized by its encoding mapping f , where

$$f : \mathcal{Q} \rightarrow \{1, 2, \dots, 2^{nBr}\}, \quad (7)$$

and its decoding mapping g , where

$$g : \{1, 2, \dots, 2^{nBr}\} \rightarrow \mathbb{R}^{nB}. \quad (8)$$

The *average distortion* between \mathbf{x} and its reconstruction $\hat{\mathbf{x}}$ is defined as

$$d(\mathbf{x}, \hat{\mathbf{x}}) \triangleq \frac{1}{nB} \sum_{i=1}^B \|\mathbf{x}_i - \hat{\mathbf{x}}_i\|_2 = \frac{1}{nB} \|\mathbf{x} - \hat{\mathbf{x}}\|_2^2, \quad (9)$$

where \mathbf{x} is defined in (6). Let $\tilde{\mathbf{x}} = g(f(\mathbf{x}))$. The distortion of code (f, g) is denoted by δ , which is defined as the supremum of all achievable average per-frame distortions. That is,

$$\delta \triangleq \sup_{\mathbf{x} \in \mathcal{Q}} d(\mathbf{x}, \tilde{\mathbf{x}}) = \sup_{\mathbf{x} \in \mathcal{Q}} \frac{1}{nB} \|\mathbf{x} - \tilde{\mathbf{x}}\|_2^2. \quad (10)$$

Let \mathcal{C} denote the codebook of this code defined as

$$\mathcal{C} = \{g(f(\mathbf{x})) : \mathbf{x} \in \mathcal{Q}\}. \quad (11)$$

Clearly, since the code is of rate r , $|\mathcal{C}| \leq 2^{nBr}$. Consider a family of compression code $\{(f_r, g_r)\}_r$ for set $\mathcal{Q} \subset \mathbb{R}^{nB}$, indexed by their rate r . The deterministic distortion-rate function of this family of codes is defined as

$$\delta(r) = \sup_{\mathbf{x} \in \mathcal{Q}} \frac{1}{nB} \|\mathbf{x} - g_r(f_r(\mathbf{x}))\|_2^2. \quad (12)$$

The corresponding deterministic rate-distortion function of this family of codes is defined as

$$r(\delta) = \inf\{r : \delta(r) \leq \delta\}.$$

The α -dimension of this family of codes is defined as [25]

$$\alpha = \limsup_{\delta \rightarrow 0} \frac{2r(\delta)}{\log \frac{1}{\delta}}. \quad (13)$$

It can be shown that in standard CS, the α -dimension of a compression code is connected to the sampling rate required for a compression-based recovery method that employs this family of codes to, asymptotically, recover the input at zero distortion [25].

Remark 1. *In our later theoretical derivations we assume that the compression code is such that $g(f(\mathbf{x}))$ returns the codeword in \mathcal{C} that is closest to \mathbf{x} . That is, $g(f(\mathbf{x})) = \operatorname{argmin}_{\mathbf{c} \in \mathcal{C}} \|\mathbf{x} - \mathbf{c}\|_2^2$.*

B. Compression-based Recovery

While the main body of research in CS has focused on structures such as sparsity and its generalizations, recently, there has been a growing body work that consider much more general structures. Given the fact that most signals of interest follow structures beyond sparsity, such new schemes potentially are more efficient in terms of their required sampling rates or reconstruction recovery.

One approach to develop recovery algorithms that employ more complex structures is to take advantage of already existing data compression codes. For some classes of signals such as images and videos, after decades of research, there exist efficient compression codes that take advantages of complex structures. Compressible signal pursuit (CSP), proposed in [25], is a compression-based recovery optimization. It proves that compression-based CS recovery is possible and can achieve the optimal performance in terms of required sampling rates.

Inspired by the CSP optimization, we propose a CSP-type optimization as a compression-based recovery algorithm for one-shot measurement systems. Consider the compact set $\mathcal{Q} \subset \mathbb{R}^{nB}$ equipped with a rate- r compression code described by mappings (f, g) , defined in (7)-(8). Consider $\mathbf{x} \in \mathcal{Q}$ and its snapshot measurement

$$\mathbf{y} = \mathbf{H}\mathbf{x} + \mathbf{z} = \sum_{i=1}^B \mathbf{D}_i \mathbf{x}_i + \mathbf{z}, \quad (14)$$

where \mathbf{H} is defined in (3) and $\mathbf{D}_i = \operatorname{diag}(D_{i1}, \dots, D_{in})$. Then, a CSP-type recovery, given \mathbf{y} and $(\mathbf{D}_1, \dots, \mathbf{D}_k)$,

estimates \mathbf{x} by solving the following optimization:

$$\hat{\mathbf{x}} = \arg \min_{\mathbf{c} \in \mathcal{C}} \left\| \mathbf{y} - \sum_{i=1}^B \mathbf{D}_i \mathbf{c}_i \right\|_2^2, \quad (15)$$

where \mathcal{C} is defined in (11). In other words, given a measurement vector \mathbf{y} , this optimization, among all compressible signals, i.e., signals in the codebook, picks the one that is closest to the observed measurements. As mentioned earlier, a key advantage of compression-based recovery methods such as (15) is that, without much additional effort, through the use of proper compression codes, they can take advantages of both temporal (spectral) and spatial dependencies that exist in multi-frame signals, such as videos. At $B = 1$, with a *traditional* dense sensing matrix, this reduces to the standard CSP optimization [25]. However, theoretically, the two setups are significantly different, and for $B > 1$, the original proof of the CSP optimization does not work in the snapshot CS setting.

The following theorem characterizes the performance of this CSP-type recovery method by connecting the parameters of the code, its rate and its distortion, to the number of frames B and the reconstruction quality.

Theorem 1. *Assume that $\forall \mathbf{x} \in \mathcal{Q}$, $\|\mathbf{x}\|_\infty \leq \frac{\rho}{2}$. Further assume the rate- r code achieves distortion δ on \mathcal{Q} . Moreover, for $i = 1, \dots, B$, $\mathbf{D}_i = \text{diag}(D_{i1}, \dots, D_{in})$, and $\{D_{ij}\}_{j=1}^n \stackrel{\text{i.i.d.}}{\sim} \mathcal{N}(0, 1)$. For $\mathbf{x} \in \mathcal{Q}$ and $\mathbf{y} = \sum_{i=1}^B \mathbf{D}_i \mathbf{x}_i$, let $\hat{\mathbf{x}}$ denote the solution of (15). Assume that $\epsilon > 0$ is a free parameter, such that $\epsilon \leq \frac{16}{3}$. Then,*

$$\frac{1}{nB} \|\mathbf{x} - \hat{\mathbf{x}}\|_2^2 \leq \delta + \rho^2 \epsilon, \quad (16)$$

with a probability larger than $1 - 2^{nBr+1} e^{-\frac{\epsilon^2 n}{16K^2}}$, where $K = 8/3$.

The proof is presented in Section V-A.

Corollary 1. *Consider the same setup as in Theorem 1. Given $\eta > 0$, assume that*

$$B < \frac{1}{\eta} \left(\frac{\log \frac{1}{\delta}}{2r} \right). \quad (17)$$

Then,

$$\Pr \left(\frac{1}{nB} \|\mathbf{x} - \hat{\mathbf{x}}\|_2^2 > \delta + 8\rho^2 \sqrt{\frac{\log \frac{1}{\delta}}{\eta}} \right) \leq 2e^{-\frac{\log \frac{1}{\delta}}{5\eta} n}, \quad (18)$$

where \log refers to logarithm in base 2.

Proof. In Theorem 1, let

$$\epsilon = 8 \sqrt{\frac{\log \frac{1}{\delta}}{\eta}}.$$

Then, according to Theorem 1, the probability of the error event can be upper bounded by

$$2^{nBr+1} e^{-\frac{\epsilon^2 n}{16K^2}} \leq 2 \exp^{-\frac{n}{\eta} \log \frac{1}{\delta} \left(\frac{4}{K^2} - \frac{\ln 2}{2} \right)}, \quad (19)$$

where $K = 8/3$. But $\frac{4}{K^2} - \frac{\ln 2}{2} > \frac{1}{5}$. Therefore, the desired result follows. \square

Consider a family of compression codes $\{(f_r, g_r)\}_r$ for set $\mathcal{Q} \subset \mathbb{R}^{nB}$, indexed by their rate r . Roughly speaking, Corollary 1 states that, as $\delta \rightarrow 0$, if B is smaller than $\frac{1}{\eta\alpha}$, where α denotes the α -dimension defined in (13), the achieved distortion by the CSP-type recovery is bounded by a constant that is inversely proportional to $\frac{1}{\sqrt{\eta}}$. (Here, η is a free parameter.) In snapshot CS, as mentioned earlier, the sampling rate is $\frac{1}{B}$. Hence, in other words, to bound the achieved distortion, this corollary requires the sampling rate to exceed $\eta\alpha$.

To better understand the α -dimension of structured multi-frame signals, consider the following set of B -frame signals in \mathbb{R}^{nB} . Assume that the first frame of each B -frame signal $\mathbf{x} \in \mathcal{Q}$ is a k -sparse signal with an ℓ_2 -norm bounded by 1, *i.e.*, $\|\mathbf{x}_1\|_2 \leq 1$ and $\|\mathbf{x}_1\|_0 \leq k$. Further assume that the next $(B-1)$ frames all share the same non-zero entries as \mathbf{x}_1 located arbitrarily across each frame. This very simple model is inspired by video frames and how consecutive frames are related to each other. Consider the following simple compression code for signals in \mathcal{Q} . For the first frame, describe the locations of the (at most k) non-zero entries and their quantized values, each quantized into a fixed number of bits. Since, by our assumption, all frames share the same non-zero values, a code for all frames can be built by just coding the locations of the non-zero entries of the remaining $(B-1)$ frames. Changing the number of bits used to quantize each non-zero element yields a family of compression codes operating at different rates and distortions. The α -dimension of the code developed for the first frame can be shown to be equal to $\frac{k}{n}$ [25]. For the code developed for B -frame signals in \mathcal{Q} , since the number of bits required for describing the locations of the non-zero entries in each frame does not depend on the selected quantization level (or δ), as $\delta \rightarrow 0$, the effect of such additional bits becomes negligible. Therefore, the α -dimension of the family of codes designed for multi-frame signals is equal to $\frac{k}{nB}$.

III. EFFICIENT COMPRESSION-BASED SNAPSHOT CS

In the previous section we discussed a compression-based for snapshot compressed sensing which was inspired by the CSP optimization. Finding the solution of this optimization requires solving a high-dimensional non-convex discrete optimization, $\min_{\mathbf{c} \in \mathcal{C}} \|\mathbf{y} - \sum_{i=1}^B \mathbf{D}_i \mathbf{c}_i\|_2^2$. Solving this optimization involves minimizing a convex cost function over exponentially many codewords. Hence, finding the solution of the CSP optimization solution through exhaustive search over the codebook is infeasible, even for small values of block-length n . To address this issue, in the following we propose two different iterative algorithms for compression-based snapshot CS that are both computationally efficient, and both achieve good performances.

A. Recovery Algorithm: Compression-based projected gradient descent

Projected gradient descent (PGD) is a well-established method for solving a convex optimization that requires minimizing a convex function subject to a convex constraint. Inspired by PGD, Algorithm 1 described below is an iterative algorithm designed to approximate the solution of the non-convex optimization described in (15). Each iteration involves two key steps:

- i) moving in the direction of the gradient of the cost function,
- ii) projecting the result onto the set of codewords.

Note that both steps are computationally very efficient. The gradient descent step involves matrix-vector multiplication, *i.e.*, $\mathbf{H}\mathbf{x}^t$ and $\mathbf{H}^\top \mathbf{e}^t$ with $\mathbf{e}^t = \mathbf{y} - \mathbf{H}\mathbf{x}^t$ and $\mathbf{H} = [\mathbf{D}_1, \dots, \mathbf{D}_B]$. The second step, the projection on the set of codewords, can be performed by applying the encoder and the decoder of the compression code.

Algorithm 1 CbPGD for Snapshot CS recovery

Require: \mathbf{H} , \mathbf{y} .

- 1: Initial $\mu > 0$, $\mathbf{x}^0 = 0$.
 - 2: **for** $t = 0$ to Max-Iter **do**
 - 3: Calculate: $\mathbf{e}^t = \mathbf{y} - \mathbf{H}\mathbf{x}^t$.
 - 4: Projected gradient descent: $\mathbf{s}^{t+1} = \mathbf{x}^t + \mu\mathbf{H}^\top \mathbf{e}^t$.
 - 5: Projection via compression: $\mathbf{x}^{t+1} = g(f(\mathbf{s}^{t+1}))$.
 - 6: **end for**
 - 7: **Output:** Reconstructed signal $\hat{\mathbf{x}}$.
-

The following theorem characterizes the performance of the proposed compression-based PGD (CbPGD) algorithm under the noiseless case, *i.e.*, $\mathbf{z} = 0$ in Eq. (14), and shows that if B is small enough, Algorithm 1 converges.

Theorem 2. Consider a compact set $\mathcal{Q} \subset \mathbb{R}^{nB}$, such that for all $\mathbf{x} \in \mathcal{Q}$, $\|\mathbf{x}\|_\infty \leq \frac{\rho}{2}$. Furthermore, consider a compression code for set \mathcal{Q} with encoding and decoding mappings, f and g , respectively, and assume that the code operates at rate r and distortion δ . Consider $\mathbf{x} \in \mathcal{Q}$, and let $\tilde{\mathbf{x}} = g(f(\mathbf{x}))$. Assume that \mathbf{x} is measured as $\mathbf{y} = \sum_{i=1}^B \mathbf{D}_i \mathbf{x}_i$, where $\mathbf{D}_i = \text{diag}(D_{i1}, \dots, D_{in})$, and $D_{ij} \stackrel{\text{i.i.d.}}{\sim} \mathcal{N}(0, 1)$. Let \mathbf{x}^t denote the output of Algorithm 1 at iteration t with $\mu = 1$. Then, given $\lambda \in (0, 0.5)$, for $t = 0, 1, \dots$, as long as $\frac{1}{nB} \|\tilde{\mathbf{x}} - \mathbf{x}^t\|_2^2 \geq \delta$, we have

$$\frac{1}{\sqrt{nB}} \|\mathbf{x}^{t+1} - \tilde{\mathbf{x}}\|_2 \leq \frac{2\lambda}{\sqrt{nB}} \|\mathbf{x}^t - \tilde{\mathbf{x}}\|_2 + 4\sqrt{\delta},$$

with a probability at least

$$1 - 2^{4nBr} e^{-\left(\frac{3\delta}{16\rho^2}\right)^2 \lambda^2 n} - (2^{2nBr} + 1) e^{-n\left(\frac{3\delta}{16\rho^2}\right)^2}. \quad (20)$$

The proof is presented in Section V-B. The following corollary is a direct result of Theorem 2.

Corollary 2. Consider the same setup as Theorem 2. Given $\lambda \in (0, 0.5)$ and $\epsilon > 0$, assume that

$$B \leq \frac{1 + \epsilon}{100r} \left(\frac{\delta\lambda}{\rho^2} \right)^2. \quad (21)$$

Then, for $t = 0, 1, \dots$, as long as $\frac{1}{nB} \|\tilde{\mathbf{x}} - \mathbf{x}^t\|_2^2 \geq \delta$, we have

$$\frac{1}{\sqrt{nB}} \|\mathbf{x}^{t+1} - \tilde{\mathbf{x}}\|_2 \leq \frac{2\lambda}{\sqrt{nB}} \|\mathbf{x}^t - \tilde{\mathbf{x}}\|_2 + 4\sqrt{\delta},$$

with a probability larger than

$$1 - e^{-\left(\frac{3\delta\lambda}{16\rho^2}\right)^2 \epsilon n}. \quad (22)$$

- Theorem 2 proves that the final distance between the recovered signal and $\tilde{\mathbf{x}}$ is bounded by a function of λ and δ , where $\tilde{\mathbf{x}}$ is the decoded version of the ground truth signal \mathbf{x} using the encoding and decoding mappings, (f, g) .
- In Theorem 2, the requirement that $\frac{1}{nB} \|\tilde{\mathbf{x}} - \mathbf{x}^t\|_2^2 \geq \delta$, while important for the proof, is a trivial assumption, as the error introduced by the compression code itself is δ . So using a lossy compression code with distortion δ , it is expected that the final distortion is larger than δ .
- Finally, in Theorem 2, the step-size is set to $\mu = 1$. However, as discussed in later in Section IV, this may not be an ideal choice in practice. In fact, in our simulations, we tune this step-size in each iteration.

Next we provide the convergence guarantee of the CbPGD algorithm in the noisy case where the measurements are corrupted by additive Gaussian noise.

Theorem 3. Consider the same setup as Theorem 2, but where the measurements are corrupted by additive noise.

That is,

$$\mathbf{y} = \sum_{i=1}^B \mathbf{D}_i \mathbf{x}_i + \mathbf{z},$$

where $\mathbf{z} = (z_1, \dots, z_n)$ and $\{z_i\}_{i=1}^n \stackrel{i.i.d.}{\sim} \mathcal{N}(0, \sigma^2)$. Then, given $\lambda \in (0, 0.5)$ and $\epsilon_z \in (0, \sqrt{\rho})$, for $t = 0, 1, \dots$, we have

$$\frac{1}{\sqrt{nB}} \|\mathbf{x}^{t+1} - \tilde{\mathbf{x}}\|_2 \leq \frac{2\lambda}{\sqrt{nB}} \|\mathbf{x}^t - \tilde{\mathbf{x}}\|_2 + 4\sqrt{\delta} + \frac{2\epsilon_z \sigma}{\sqrt{B}},$$

with a probability larger than

$$1 - 2^{4nBr} e^{-\left(\frac{3\delta}{16\rho^2}\right)^2 \lambda^2 n} - (2^{2nBr} + 1) e^{-n\left(\frac{3\delta}{16\rho^2}\right)^2} - 2^{2nBr} e^{-n\left(\frac{3\epsilon_z}{16\rho}\right)^2 \delta}. \quad (23)$$

The proof is presented in Section V-C.

Remark 2. It can be seen from Theorem 2 and Theorem 3 that in the noisy case, the convergence rate of CbPGD is slower and it is dependent on the power of the noise; meanwhile, the probability is also smaller than that of

noiseless case.

B. Compression-based generalized alternating projection

In the previous section we studied convergence performance of the CbPGD algorithm for a fixed μ . However, in practice, to implement CbPGD, one key step is to tune the step size μ . This step is usually time-consuming and the performance is sensitive on the choice of μ . In order to mitigate this issue, and due to the special structure of the sensing matrix, which makes $\mathbf{H}\mathbf{H}^\top$ a diagonal matrix, inspired by the generalized alternating projection (GAP) [40] algorithm, we propose a compression-based GAP (CbGAP) recovery algorithm for snapshot CS in Algorithm 2. Here, as before, $\mathbf{H} = [\mathbf{D}_1, \dots, \mathbf{D}_B]$, where $\mathbf{D}_i = \text{diag}(D_{i1}, \dots, D_{in})$ denotes the sensing matrix. Matrix \mathbf{R} is defined as

$$\mathbf{R} = \mathbf{H}\mathbf{H}^\top = \text{diag}(R_1, \dots, R_n), \quad (24)$$

where $R_j = \sum_{i=1}^B D_{ij}^2, \forall j = 1, \dots, n$. Note that the $\mathbf{R}^{-1}\mathbf{e}^t$ in the Euclidean projection step of Algorithm 2 can be computed element-wise and thus is very efficient. Moreover, during the implementation, we never store $\{\mathbf{D}_i\}_{i=1}^B$ and \mathbf{R} , but only their diagonal elements.

Algorithm 2 CbGAP for Snapshot CS recovery

Require: \mathbf{H}, \mathbf{y} .

- 1: Initial $\mu > 0, \mathbf{x}^0 = 0$.
 - 2: **for** $t = 0$ to Max-Iter **do**
 - 3: Calculate: $\mathbf{e}^t = \mathbf{y} - \mathbf{H}\mathbf{x}^t$.
 - 4: Euclidean projection: $\mathbf{s}^{t+1} = \mathbf{x}^t + \mu\mathbf{H}^\top\mathbf{R}^{-1}\mathbf{e}^t$.
 - 5: Projection via compression: $\mathbf{x}^{t+1} = g(f(\mathbf{s}^{t+1}))$.
 - 6: **end for**
 - 7: **Output:** Reconstructed signal $\hat{\mathbf{x}}$.
-

The following theorem characterizes the convergence performance of the described compression-based GAP algorithm. Similar to Theorem 2, the following theorem proves that if B is small enough, Algorithm 2 converges.

Theorem 4. *Consider the same setting as Theorem 2. For $t = 0, 1, \dots$, let $\mathbf{s}^{t+1} = \mathbf{x}^t + B\mathbf{H}^\top\mathbf{R}^{-1}(\mathbf{y} - \mathbf{H}\mathbf{x}^t)$, and $\mathbf{x}^{t+1} = g(f(\mathbf{s}^{t+1}))$, where $\mathbf{R} = \mathbf{H}\mathbf{H}^\top$. Then, given $\lambda \in (0, 0.5)$, for $t = 0, 1, \dots$, as long as $\frac{1}{nB}\|\tilde{\mathbf{x}} - \mathbf{x}^t\|_2^2 \geq \delta$, we have*

$$\frac{1}{\sqrt{nB}}\|\mathbf{x}^{t+1} - \tilde{\mathbf{x}}\|_2 \leq \frac{2\lambda}{\sqrt{nB}}\|\mathbf{x}^t - \tilde{\mathbf{x}}\|_2 + 4\sqrt{\delta},$$

with a probability at least

$$1 - 2^{4nBr}e^{-\frac{\lambda^2\delta^2n}{2B\rho^4}} - 2^{2nBr}e^{-\frac{n\delta}{2\rho^2B^2}}. \quad (25)$$

The proof is presented in Section V-D.

- Theorem 2 and Theorem 4 show that CbGAP and CbPGD have very similar convergence behaviors. Moreover, the important message of both results is the following: for a fixed $\lambda > 0$, (20) and (25) bound the number of frames (B) that can be combined together, and still be recovered by the CbPGD algorithm and the CbGAP algorithm, respectively, as a function of λ , δ , r , and ρ .
- Though Theorem 4 proves the convergence of GAP when $\mu = B$, in our simulations and in real applications, we found that $\mu \in \{1, 2\}$ always leads to better results. By contrast, in CbPGD, $\mu = 2/B$ is usually a good choice for a fixed step-size.

IV. SIMULATION RESULTS

As mentioned in Section I-A, snapshot CS is used in various applications. As a widely used example, in this section, we report our simulation results for video CS and compare the performances of our proposed compression-based PGD and GAP algorithms with leading algorithms⁴, i.e., GMM [26], [27], GAP-wavelet-tree [18], and GAP-TV [43] with sources codes downloaded from the authors’ websites. All algorithms are performed in MATLAB.

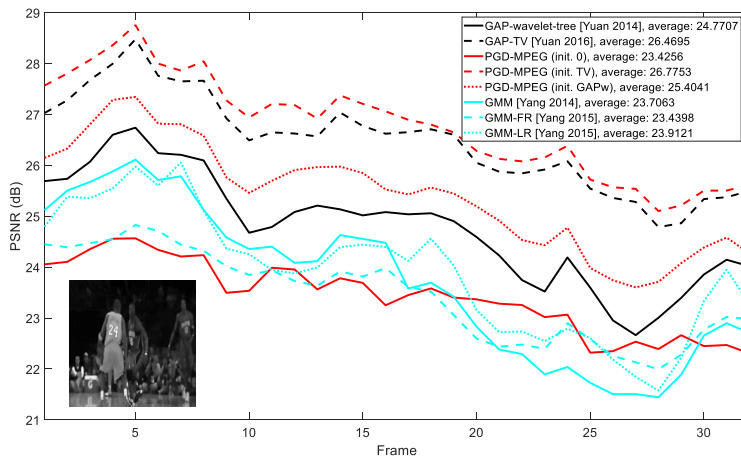


Fig. 1. PSNR curves of reconstructed video frames compared with ground truth using different algorithms. $B = 8$ with 4 measurements.

A. MPEG Video Compression

In the first set of experiments we use the MPEG [44] video compression algorithm inside the compression-based PGD algorithm described in Algorithm 1. Thus we refer to the resulting recovery method as “PGD-MPEG”. Different initialization approaches are used in our algorithms, where “PGD-MPEG (init. 0)” denotes initializing with zeros, “PGD-MPEG (init. TV)” signifies the GAP-TV results are used as initialization, and “PGD-MPEG (init. GAPw)”

⁴Most recently, the deep learning techniques have been employed for video CS [41], [42]. We are not aiming to compete with these advanced algorithms as they are usually complicated and require data to train the neural networks. Furthermore, some of these algorithms require the sensing matrix being spatially repetitive.

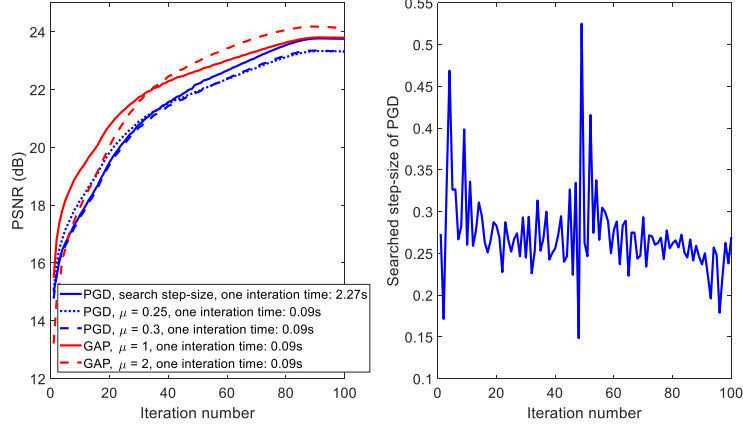


Fig. 2. Left: PSNR of reconstructed video frames using GAP and PGD at each iteration. Right: The searched step size of PGD.

uses the GAP-wavelet-tree results for initialization. Fig. 1 plots the PSNR curves of different algorithms versus the frame number on the *Kobe* dataset used in [26]. Following the set up in [26], the video frame size is of 256×256 pixels. $B = 8$ video frames are modulated and collapsed into a single 256×256 snapshot measurement. There are in total 32 frames and thus 4 measured frames are available. For each measured frame, given the masks, i.e., the sensing matrices $\{\mathbf{D}_i\}_{i=1}^B$, which are generated once and used in all algorithms, the task is to reconstruct the eight video frames. The peak-signal-to-noise-ratio (PSNR) is employed as the metric to compare different algorithms. It can be seen that, even initializing with zeros, the performance of PGD-MPEG is comparable with GMM, GMM-LR and GMM-FR [27]. When initializing with the results of other algorithms, PGD-MPEG can boost the PSNR up by more than 0.3dB. While the GMM-based algorithms are usually slow, GAP-TV provides a descent result in a few seconds. Therefore, it is reasonable to initialize the PGD algorithm by the results of GAP-TV. Regarding the computation time of our algorithm, for the mentioned parameters, it takes around 10 seconds for GAP-MPEG to provide decent results, which is further validated in Fig. 2.

In our PGD algorithm reported in Fig. 1, we search the step-size in each iteration via minimizing the measurement error. Specifically, let μ_t denote the step-size at t^{th} iteration of PGD. We set μ_t by solving

$$\mu_t = \underset{\mu}{\operatorname{argmin}} \|\mathbf{y} - \mathbf{H}[g(f(\mathbf{x}^t + \mu\mathbf{H}^\top(\mathbf{y} - \mathbf{H}\mathbf{x}^t)))]\|_2. \quad (26)$$

In this way, the next estimate is moved as close as possible to the manifold $\mathcal{M} = \{\xi | \mathbf{y} = \mathbf{H}\xi\}$. We employ derivative-free methods, such as [45], to solve this optimization problem. However, this is still time consuming. We thus report the performance of our proposed fixed step-size algorithm, namely GAP. In Fig. 2, we plot the reconstruction PSNRs of both (fixed step-size) GAP and (step-size-optimized) PGD versus iteration number. It can be seen that GAP and PGD converge to the similar level within 100 iterations. Since no step-size search is required, one iteration of GAP only takes 0.09 seconds, which is more than 280 times faster than PGD, which searches for

TABLE I
PSNR (dB) OF RECONSTRUCTED VIDEOS USING DIFFERENT ALGORITHMS

Algorithm	Kobe	Traffic	Runner
GAP-TV [43]	26.47	20.17	30.05
GAP-wavelet-tree [18]	24.77	21.16	25.61
GMM [26]	23.71	21.03	29.03
GMM-FR [27]	23.44	21.84	33.16
GMM-LR [27]	23.91	21.09	30.70
GAP-MPEG	26.78	21.78	31.02
GAP-NLS	28.00	24.56	37.18

the right step-size. We also plot the results of PGD by different step-sizes, i.e., $\mu = \{0.25, 0.3\}$, and the results are worse than that of PGD by optimizing step-size. They are also worse than GAP at $\mu = 1$. When $\mu = 2$, GAP can provide better results, i.e., 0.3dB higher PSNR. We can notice that GAP employs a different step-size on each measurement element by $\{R_j\}_{j=1}^n$ even using the same μ , while PGD is trying to search the optimum one for all measurement elements.

B. Customized Video Compression

MPEG video compression involves performing two key steps: JPEG compression of the intra-frames (I-frames) and motion compensation, which exploits the temporal dependencies between different frames. One drawback of the JPEG-based MPEG compression is that, since it relies on discrete Cosine transformation (DCT) of individual local patches, it does not exploit *nonlocal* similarities [46] (The most recent video Codec, e.g., H.265/266 considers the similarities between patches but the patches need to be connected, thus local similarity). Using nonlocal similarities in images or videos can potentially improve the performance significantly and this has been observed in various applications [31], [47], [48].

One advantage of our proposed snapshot CS algorithms is that they can readily be combined with any (off-the-shelf or newly-designed) compression codes. Hence, motivated by the aforementioned nonlocal similarity, we describe a compression-decompression code that takes advantage of such structures. Note that to employ a compression code within either of our algorithms, we only need to have access to the combined $g(f(\mathbf{x}))$ mapping, for any $\mathbf{x} \in \mathbb{R}^{nB}$, and not $f(\mathbf{x})$ itself. Hence, to describe our proposed compression code, we mainly focus on this mapping from input to its lossy reconstruction. The details of the code can be found in Appendix A. The key operation of the proposed code is the following: given a B -frame video $\{\mathbf{x}_i\}_{i=1}^B$ signal, using a small square window, it crawls over the first frame and considers all 3D blocks that result by considering the image of each block across the remaining $(B - 1)$ frames. Then the similarities between these 3D blocks are measured and “similar” blocks are grouped together. After this, group-sparsity principles [49], [50] are used to encode such groups of blocks, which shares the same spirit with vBM4D [48].

Combining the described code with the CbGAP method (Algorithm 2) results in an algorithm which we refer to as ‘‘GAP-NLS’’ (GAP with nonlocal structure). To evaluate the performance of GAP-NLS, in addition to the `Kobe` dataset used in Fig. 1, we also consider the `Traffic` dataset used in [26] and the `Runner` dataset from [51]. Table I summarizes the video reconstruction results of our proposed method (GAP-NLS) compared with GAP-MPEG and other algorithms for these three videos. It can be observed that GAP-NLS yields the best results; it achieves more than $\{1.5\text{dB}, 2.7\text{dB}, 4\text{dB}\}$ higher PSNR compared with the best result achieved by other algorithms on `Kobe`, `Traffic`, and `Runner` datasets, respectively. The reconstructed video frames can be found in Fig. 3. Since the encoder here is more complicated than MPEG, each iteration costs about 3 seconds in our MATLAB implementation. Therefore, if a fast result is desired, GAP-MPEG is recommended and GAP-NLS is the best fit for high accuracy reconstruction.

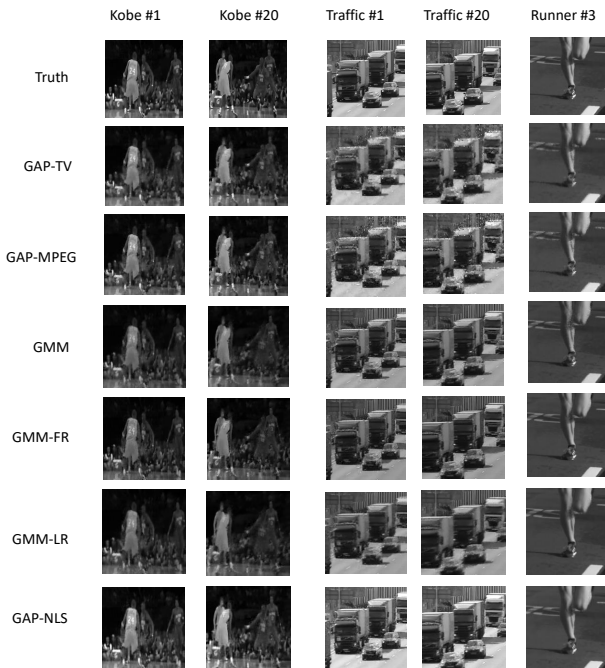


Fig. 3. Reconstructed video frames of three datasets compared with group truth using different algorithms (shown on left).

V. PROOFS OF THE MAIN RESULTS

Before presenting the proof, we first review some known results on the concentration of sub-Gaussian and sub-exponential random variables. These results are used throughout the proofs.

Definition 1. A random variable X is sub-Gaussian when

$$\|X\|_{\psi_2} \triangleq \inf \left\{ L > 0 : \mathbb{E} \left[\exp \left(\frac{|X|^2}{L^2} \right) \right] \leq 2 \right\} < \infty.$$

For a normal random variable $X \sim \mathcal{N}(0, \sigma^2)$, it is straightforward to show that $\|X\|_{\psi_2} = \sqrt{\frac{2}{3}}\sigma$.

Definition 2. A random variable X is a sub-exponential random variable, if

$$\|X\|_{\psi_1} \triangleq \inf \left\{ L > 0 : \mathbb{E} \left[e^{\frac{|X|}{L}} \right] \leq 2 \right\} < \infty.$$

Lemma 1. If X and Y be sub-Gaussian random variables, then XY is sub-exponential, and $\|XY\|_{\psi_1} \leq \|X\|_{\psi_2} \|Y\|_{\psi_2}$.

Theorem 5 (Bernstein Type Inequality, see e.g.[52]). Consider independent random variables $\{X_i\}_{i=1}^n$, where for $i = 1, \dots, n$, X_i is a sub-exponential random variable. Let $\max_i \|X_i\|_{\psi_1} \leq K$, for some $K > 0$. Then for every $t \geq 0$ and every $\mathbf{w} = [w_1, \dots, w_n]^T \in \mathbb{R}^{n \times 1}$, we have

$$\begin{aligned} & \Pr \left(\sum_{i=1}^n w_i (X_i - \mathbb{E}[X_i]) \geq t \right) \\ & \leq \exp \left\{ - \min \left(\frac{t^2}{4K^2 \|\mathbf{w}\|_2^2}, \frac{t}{2K \|\mathbf{w}\|_\infty} \right) \right\}. \end{aligned} \quad (27)$$

A. Proof of Theorem 1

Proof. Let $\tilde{\mathbf{x}} = g(f(\mathbf{x}))$. By assumption the code operates at distortion δ . Hence, $\frac{1}{nB} \|\mathbf{x} - \tilde{\mathbf{x}}\|_2^2 \leq \delta$. Moreover, since $\hat{\mathbf{x}} = \arg \min_{\mathbf{c} \in \mathcal{C}} \left\| \mathbf{y} - \sum_{i=1}^B \mathbf{D}_i \mathbf{c}_i \right\|_2^2$ and $\tilde{\mathbf{x}} \in \mathcal{C}$, we have

$$\left\| \mathbf{y} - \sum_{i=1}^B \mathbf{D}_i \hat{\mathbf{x}}_i \right\|_2^2 \leq \left\| \mathbf{y} - \sum_{i=1}^B \mathbf{D}_i \tilde{\mathbf{x}}_i \right\|_2^2,$$

or, since $\mathbf{y} = \sum_{i=1}^B \mathbf{D}_i \mathbf{x}_i$,

$$\left\| \sum_{i=1}^B \mathbf{D}_i (\mathbf{x}_i - \hat{\mathbf{x}}_i) \right\|_2^2 \leq \left\| \sum_{i=1}^B \mathbf{D}_i (\mathbf{x}_i - \tilde{\mathbf{x}}_i) \right\|_2^2. \quad (28)$$

Given $\epsilon_1 > 0$ and $\epsilon_2 > 0$ and $\mathbf{x} \in \mathbb{R}^{Bn}$, define events \mathcal{E}_1 and \mathcal{E}_2 as

$$\left\{ \frac{1}{n} \left\| \sum_{i=1}^B \mathbf{D}_i (\mathbf{x}_i - \mathbf{c}_i) \right\|_2^2 \leq \frac{1}{n} \|\mathbf{x} - \mathbf{c}\|_2^2 + B\rho^2 \epsilon_1 : \forall \mathbf{c} \in \mathcal{C} \right\} \quad (29)$$

and

$$\left\{ \frac{1}{n} \left\| \sum_{i=1}^B \mathbf{D}_i (\mathbf{x}_i - \mathbf{c}_i) \right\|_2^2 \geq \frac{1}{n} \|\mathbf{x} - \mathbf{c}\|_2^2 - B\rho^2 \epsilon_2 : \forall \mathbf{c} \in \mathcal{C} \right\}, \quad (30)$$

respectively. Then, conditioned on $\mathcal{E}_1 \cap \mathcal{E}_2$, since $\hat{\mathbf{x}} \in \mathcal{C}$ and $\tilde{\mathbf{x}} \in \mathcal{C}$, it follows from (28) that

$$\frac{1}{n} \|\mathbf{x} - \hat{\mathbf{x}}\|_2^2 \leq \frac{1}{n} \|\mathbf{x} - \tilde{\mathbf{x}}\|_2^2 + B\rho^2 \epsilon_1 + B\rho^2 \epsilon_2. \quad (31)$$

In the rest of the proof, we focus on bounding $P(\mathcal{E}_1^c \cup \mathcal{E}_2^c)$. Note that, for a fixed $\mathbf{c} \in \mathcal{C}$,

$$\left\| \sum_{i=1}^B \mathbf{D}_i(\mathbf{x}_i - \tilde{\mathbf{c}}_i) \right\|_2^2 = \sum_{j=1}^n \left(\sum_{i=1}^B D_{ij}(x_{ij} - c_{ij}) \right)^2. \quad (32)$$

Note that, for $j = 1, \dots, n$, $\sum_{i=1}^B \mathbf{D}_i(x_{ij} - c_{ij})$ are independent zero-mean Gaussian random variables. Moreover,

$$\begin{aligned} & \mathbb{E} \left[\left(\sum_{i=1}^B D_{ij}(x_{ij} - c_{ij}) \right)^2 \right] \\ &= \mathbb{E} \left[\sum_{i=1}^B \sum_{i'=1}^B D_{ij} D_{i'j} (x_{ij} - c_{ij})(x_{i'j} - c_{i'j}) \right] \\ &= \sum_{i=1}^B (x_{ij} - c_{ij})^2. \end{aligned} \quad (33)$$

For $j = 1, \dots, n$, define

$$w_j \triangleq \sum_{i=1}^B (x_{ij} - c_{ij})^2, \quad (34)$$

and

$$Z_j \triangleq \frac{\sum_{i=1}^B D_{ij}(x_{ij} - c_{ij})}{\sqrt{\sum_{i=1}^B (x_{ij} - c_{ij})^2}}. \quad (35)$$

Note that Z_1, \dots, Z_n are i.i.d. $\mathcal{N}(0, 1)$ random variables. Then, $\left\| \sum_{i=1}^B \mathbf{D}_i(\mathbf{x}_i - \mathbf{c}_i) \right\|_2^2$ can be written as $\sum_{j=1}^n w_j Z_j^2$.

But

$$\sum_{j=1}^n w_j = \sum_{j=1}^n \sum_{i=1}^B (x_{ij} - c_{ij})^2 = \|\mathbf{x} - \mathbf{c}\|_2^2.$$

Therefore, for a fixed $\mathbf{c} \in \mathcal{C}$,

$$\begin{aligned} & \Pr \left(\frac{1}{n} \left\| \sum_{i=1}^B \mathbf{D}_i(\mathbf{x}_i - \mathbf{c}_i) \right\|_2^2 \geq \frac{1}{n} \|\mathbf{x} - \mathbf{c}\|_2^2 + B\rho^2\epsilon_1 \right) \\ &= \Pr \left(\frac{1}{n} \sum_{j=1}^n w_j (Z_j^2 - 1) \geq B\rho^2\epsilon_1 \right), \end{aligned} \quad (36)$$

where w_j and Z_j are defined in (34) and (35), respectively. As proved earlier, Z_1, \dots, Z_n are i.i.d. $\mathcal{N}(0, 1)$. Also, for all $j = 1, \dots, n$, $\|Z_j^2\|_{\psi_1} \leq \|Z_j\|_{\psi_2}^2 \leq \frac{8}{3}$. Therefore, it follows from Theorem 5 that

$$\begin{aligned} & \Pr \left(\frac{1}{n} \left\| \sum_{i=1}^B \mathbf{D}_i(\mathbf{x}_i - \mathbf{c}_i) \right\|_2^2 \geq \frac{1}{n} \|\mathbf{x} - \mathbf{c}\|_2^2 + B\rho^2\epsilon_1 \right) \\ & \leq \exp \left\{ - \min \left(\frac{n^2 B^2 \rho^4 \epsilon_1^2}{4K^2 \|\mathbf{w}\|_2^2}, \frac{nB\rho^2\epsilon_1}{2K \|\mathbf{w}\|_\infty} \right) \right\}, \end{aligned} \quad (37)$$

where $K = \frac{\rho}{\epsilon_1}$. Similarly, for fixed \mathbf{x} and \mathbf{c} ,

$$\begin{aligned} \Pr \left(\frac{1}{n} \left\| \sum_{i=1}^B \mathbf{D}_i (\mathbf{x}_i - \mathbf{c}_i) \right\|_2^2 \leq \frac{1}{n} \|\mathbf{x} - \mathbf{c}\|_2^2 - B\rho^2\epsilon_2 \right) \\ \leq \exp \left\{ - \min \left(\frac{n^2 B^2 \rho^4 \epsilon_2^2}{4K^2 \|\mathbf{w}\|_2^2}, \frac{nB\rho^2\epsilon_2}{2K \|\mathbf{w}\|_\infty} \right) \right\}. \end{aligned} \quad (38)$$

The final result follows by the union bound, and the fact that $|\mathcal{C}| \leq 2^{nBr}$. Note that $\|\mathbf{w}\|_1 = \sum_{j=1}^n w_j = \sum_{j=1}^n \sum_{i=1}^B (x_{ij} - c_{ij})^2 = \|\mathbf{x} - \mathbf{c}\|_2^2$. Furthermore, since by assumption the ℓ_∞ -norms of all signals in \mathcal{Q} are upper-bounded by $\rho/2$, we have

$$\begin{aligned} \|\mathbf{w}\|_2^2 &= \sum_{j=1}^n w_j^2 = \sum_{j=1}^n \left(\sum_{i=1}^B (x_{ij} - c_{ij})^2 \right)^2 \\ &\leq \sum_{j=1}^n \left(\sum_{i=1}^B \left(\frac{\rho}{2} + \frac{\rho}{2} \right)^2 \right)^2 = B^2 \rho^4 n, \end{aligned} \quad (39)$$

and

$$\|\mathbf{w}\|_\infty = \max_{j=1, \dots, n} \sum_{i=1}^B (x_{ij} - c_{ij})^2 \leq B\rho^2. \quad (40)$$

Therefore, combining (39) and (40) with (37) and (38), it follows that

$$\begin{aligned} \Pr \left(\frac{1}{n} \left\| \sum_{i=1}^B \mathbf{D}_i (\mathbf{x}_i - \mathbf{c}_i) \right\|_2^2 \geq \frac{1}{n} \|\mathbf{x} - \mathbf{c}\|_2^2 + B\rho^2\epsilon_1 \right) \\ \leq \exp \left\{ - \min \left(\frac{n\epsilon_1^2}{4K^2}, \frac{n\epsilon_1}{2K} \right) \right\}, \end{aligned} \quad (41)$$

and

$$\begin{aligned} \Pr \left(\frac{1}{n} \left\| \sum_{i=1}^B \mathbf{D}_i (\mathbf{x}_i - \mathbf{c}_i) \right\|_2^2 \leq \frac{1}{n} \|\mathbf{x} - \mathbf{c}\|_2^2 - B\rho^2\epsilon_2 \right) \\ \leq \exp \left\{ - \min \left(\frac{n\epsilon_2^2}{4K^2}, \frac{n\epsilon_2}{2K} \right) \right\}, \end{aligned} \quad (42)$$

respectively. Assume that $\max(\epsilon_1, \epsilon_2) \leq 2K$. Then, $\min\left(\frac{\epsilon_1}{2K}, 1\right) = \frac{\epsilon_1}{2K}$ and $\min\left(\frac{B\epsilon_2}{2K}, 1\right) = \frac{\epsilon_2}{2K}$. Hence,

$$\begin{aligned} \Pr \left(\frac{1}{n} \left\| \sum_{i=1}^B \mathbf{D}_i (\mathbf{x}_i - \mathbf{c}_i) \right\|_2^2 \geq \frac{1}{n} \|\mathbf{x} - \mathbf{c}\|_2^2 + B\rho^2\epsilon_1 \right) \\ \leq \exp \left\{ - \frac{n\epsilon_1^2}{4K^2} \right\}, \end{aligned} \quad (43)$$

and

$$\begin{aligned} \Pr \left(\frac{1}{n} \left\| \sum_{i=1}^B \mathbf{D}_i (\mathbf{x}_i - \mathbf{c}_i) \right\|_2^2 \leq \frac{1}{n} \|\mathbf{x} - \mathbf{c}\|_2^2 - B\rho^2\epsilon_2 \right) \\ \leq \exp \left\{ -\frac{n\epsilon_2^2}{4K^2} \right\}. \end{aligned} \quad (44)$$

To finish the proof note that $|\mathcal{C}| \leq 2^{nBr}$. Therefore, by the union bound,

$$\Pr(\mathcal{E}_1^c) \leq 2^{nBr} \exp \left\{ -\frac{n\epsilon_1^2}{4K^2} \right\}, \quad (45)$$

and

$$\Pr(\mathcal{E}_2^c) \leq 2^{nBr} \exp \left\{ -\frac{n\epsilon_2^2}{4K^2} \right\}. \quad (46)$$

Finally, again by the union bound, $P(\mathcal{E}_1 \cap \mathcal{E}_2) \geq 1 - P(\mathcal{E}_1^c) - P(\mathcal{E}_2^c)$. Given $0 < \epsilon < \frac{16}{3}$, the desired result follows by letting $\epsilon_1 = \epsilon_2 = \epsilon/2$. Plug this into (31), we have

$$\frac{1}{n} \|\mathbf{x} - \hat{\mathbf{x}}\|_2^2 \leq \frac{1}{n} \|\mathbf{x} - \tilde{\mathbf{x}}\|_2^2 + B\rho^2\epsilon \leq B\delta + B\rho^2\epsilon. \quad (47)$$

This is

$$\frac{1}{nB} \|\mathbf{x} - \hat{\mathbf{x}}\|_2^2 \leq \delta + \rho^2\epsilon. \quad (48)$$

Also, from (45) and (46), for $\epsilon_1 = \epsilon_2 = \epsilon/2$,

$$\begin{aligned} \Pr(\mathcal{E}_1 \cap \mathcal{E}_2) &\geq 1 - 2^{nBr} \exp \left\{ -\frac{n\epsilon_1^2}{4K^2} \right\} - 2^{nBr} \exp \left\{ -\frac{n\epsilon_2^2}{4K^2} \right\} \\ &= 1 - 2^{nBr+1} \exp \left\{ -\frac{n\epsilon^2}{16K^2} \right\}. \end{aligned} \quad (49)$$

□

B. Proof of Theorem 2

Proof. At step t , given \mathbf{x}^t , define the error vector and its normalized version as

$$\boldsymbol{\theta}^t = \tilde{\mathbf{x}} - \mathbf{x}^t, \quad (50)$$

and

$$\bar{\boldsymbol{\theta}}^t = \frac{\boldsymbol{\theta}^t}{\|\boldsymbol{\theta}^t\|_2}, \quad (51)$$

respectively. By this definition, for $i = 1, \dots, B$, the i -th block of each of these error vectors can be written as $\mathbf{e}_i^t = \tilde{\mathbf{x}}_i - \mathbf{x}_i^t$, and

$$\bar{\boldsymbol{\theta}}_i^t = \frac{\tilde{\mathbf{x}}_i - \mathbf{x}_i^t}{\|\tilde{\mathbf{x}} - \mathbf{x}^t\|_2}.$$

Moreover, by assumption 6),

$$\frac{1}{nB} \sum_{i=1}^B \|\tilde{\mathbf{x}}_i - \mathbf{x}_i^t\|_2^2 \geq \delta,$$

Therefore, $\min(\|\boldsymbol{\theta}^t\|_2^2, \|\boldsymbol{\theta}^{t+1}\|_2^2) \geq nB\delta$.

For $i = 1, \dots, B$ and $j = 1, \dots, n$, since for all $\mathbf{x} \in \mathcal{Q}$, $\|\mathbf{x}\|_\infty \leq \frac{\rho}{2}$, we have

$$|\bar{\theta}_{ij}^t|^2 = \frac{(\tilde{x}_{ij} - x_{ij}^t)^2}{\|\boldsymbol{\theta}^t\|_2^2} \leq \frac{\rho^2}{nB\delta} \quad (52)$$

and, similarly,

$$|\bar{\theta}_{ij}^{t+1}|^2 \leq \frac{\rho^2}{nB\delta} \quad (53)$$

Since \mathbf{x}^{t+1} is the closest codeword to \mathbf{s}^{t+1} in \mathcal{C} , and $\tilde{\mathbf{x}}$ is also in \mathcal{C} , it follows that $\|\mathbf{s}^{t+1} - \mathbf{x}^{t+1}\|_2^2 \leq \|\mathbf{s}^{t+1} - \tilde{\mathbf{x}}\|_2^2$, or

$$\sum_{i=1}^B \|\mathbf{s}_i^{t+1} - \mathbf{x}_i^{t+1}\|_2^2 \leq \sum_{i=1}^B \|\mathbf{s}_i^{t+1} - \tilde{\mathbf{x}}_i\|_2^2. \quad (54)$$

But

$$\begin{aligned} \|\mathbf{s}_i^{t+1} - \mathbf{x}_i^{t+1}\|_2^2 &= \|\mathbf{s}_i^{t+1} - \tilde{\mathbf{x}}_i + \tilde{\mathbf{x}}_i - \mathbf{x}_i^{t+1}\|_2^2 \\ &= \|\mathbf{s}_i^{t+1} - \tilde{\mathbf{x}}_i\|_2^2 + 2\langle \mathbf{s}_i^{t+1} - \tilde{\mathbf{x}}_i, \tilde{\mathbf{x}}_i - \mathbf{x}_i^{t+1} \rangle + \|\tilde{\mathbf{x}}_i - \mathbf{x}_i^{t+1}\|_2^2. \end{aligned} \quad (55)$$

Therefore, along with (54),

$$\begin{aligned} \|\mathbf{s}_i^{t+1} - \tilde{\mathbf{x}}_i\|_2^2 + 2\langle \mathbf{s}_i^{t+1} - \tilde{\mathbf{x}}_i, \tilde{\mathbf{x}}_i - \mathbf{x}_i^{t+1} \rangle + \|\tilde{\mathbf{x}}_i - \mathbf{x}_i^{t+1}\|_2^2 \\ \leq \|\mathbf{s}_i^{t+1} - \tilde{\mathbf{x}}_i\|_2^2. \end{aligned} \quad (56)$$

This is

$$\begin{aligned}
& \sum_{i=1}^B \|\tilde{\mathbf{x}}_i - \mathbf{x}_i^{t+1}\|_2^2 \leq 2 \sum_{i=1}^B \langle \tilde{\mathbf{x}}_i - \mathbf{s}_i^{t+1}, \tilde{\mathbf{x}}_i - \mathbf{x}_i^{t+1} \rangle \\
& \stackrel{(a)}{=} 2 \sum_{i=1}^B \langle \tilde{\mathbf{x}}_i - \mathbf{x}_i^t - \mathbf{D}_i \mathbf{e}^t, \tilde{\mathbf{x}}_i - \mathbf{x}_i^{t+1} \rangle \\
& \stackrel{(b)}{=} 2 \sum_{i=1}^B \langle \tilde{\mathbf{x}}_i - \mathbf{x}_i^t, \tilde{\mathbf{x}}_i - \mathbf{x}_i^{t+1} \rangle \\
& \quad - 2 \sum_{i=1}^B \left\langle \mathbf{D}_i \left(\mathbf{y} - \sum_{j=1}^B \mathbf{D}_j \mathbf{x}_j^t \right), \tilde{\mathbf{x}}_i - \mathbf{x}_i^{t+1} \right\rangle \\
& = 2 \sum_{i=1}^B \langle \tilde{\mathbf{x}}_i - \mathbf{x}_i^t, \tilde{\mathbf{x}}_i - \mathbf{x}_i^{t+1} \rangle \\
& \quad - 2 \left\langle \sum_{j=1}^B \mathbf{D}_j (\mathbf{x}_j - \mathbf{x}_j^t), \sum_{i=1}^B \mathbf{D}_i (\tilde{\mathbf{x}}_i - \mathbf{x}_i^{t+1}) \right\rangle \\
& = 2 \sum_{i=1}^B \langle \tilde{\mathbf{x}}_i - \mathbf{x}_i^t, \tilde{\mathbf{x}}_i - \mathbf{x}_i^{t+1} \rangle \\
& \quad - 2 \left\langle \sum_{i=1}^B \mathbf{D}_i (\mathbf{x}_i - \tilde{\mathbf{x}}_i + \tilde{\mathbf{x}}_i - \mathbf{x}_i^t), \sum_{i=1}^B \mathbf{D}_i (\tilde{\mathbf{x}}_i - \mathbf{x}_i^{t+1}) \right\rangle \\
& = 2 \sum_{i=1}^B \langle \tilde{\mathbf{x}}_i - \mathbf{x}_i^t, \tilde{\mathbf{x}}_i - \mathbf{x}_i^{t+1} \rangle \\
& \quad - 2 \left\langle \sum_{i=1}^B \mathbf{D}_i (\tilde{\mathbf{x}}_i - \mathbf{x}_i^t), \sum_{i=1}^B \mathbf{D}_i (\tilde{\mathbf{x}}_i - \mathbf{x}_i^{t+1}) \right\rangle \\
& \quad - 2 \left\langle \sum_{i=1}^B \mathbf{D}_i (\mathbf{x}_i - \tilde{\mathbf{x}}_i), \sum_{i=1}^B \mathbf{D}_i (\tilde{\mathbf{x}}_i - \mathbf{x}_i^{t+1}) \right\rangle. \tag{57}
\end{aligned}$$

where (a) and (b) follow from $\mathbf{e}^t = \mathbf{y} - \sum_{i=1}^B \mathbf{D}_i \mathbf{x}_i^t$ and $\mathbf{s}_i^{t+1} = \mathbf{x}_i^t + \mathbf{D}_i \mathbf{e}^t$, respectively. Then, using $\bar{\boldsymbol{\theta}}^t$ and $\bar{\boldsymbol{\theta}}^{t+1}$ defined in (51), the first two terms at the end of (57) can be written as

$$\begin{aligned}
& 2 \sum_{i=1}^B \langle \tilde{\mathbf{x}}_i - \mathbf{x}_i^t, \tilde{\mathbf{x}}_i - \mathbf{x}_i^{t+1} \rangle \\
& \quad - 2 \left\langle \sum_{i=1}^B \mathbf{D}_i (\tilde{\mathbf{x}}_i - \mathbf{x}_i^t), \sum_{i=1}^B \mathbf{D}_i (\tilde{\mathbf{x}}_i - \mathbf{x}_i^{t+1}) \right\rangle \\
& = 2 \|\bar{\boldsymbol{\theta}}^t\|_2 \|\bar{\boldsymbol{\theta}}^{t+1}\|_2 \left(\sum_{i=1}^B \langle \bar{\boldsymbol{\theta}}_i^t, \bar{\boldsymbol{\theta}}_i^{t+1} \rangle - \left\langle \sum_{i=1}^B \mathbf{D}_i \bar{\boldsymbol{\theta}}_i^t, \sum_{i=1}^B \mathbf{D}_i \bar{\boldsymbol{\theta}}_i^{t+1} \right\rangle \right). \tag{58}
\end{aligned}$$

And

$$\begin{aligned}
& \sum_{i=1}^B \langle \bar{\boldsymbol{\theta}}_i^t, \bar{\boldsymbol{\theta}}_i^{t+1} \rangle - \left\langle \sum_{i=1}^B \mathbf{D}_i \bar{\boldsymbol{\theta}}_i^t, \sum_{i=1}^B \mathbf{D}_i \bar{\boldsymbol{\theta}}_i^{t+1} \right\rangle \\
&= \sum_{j=1}^n \left(\sum_{i=1}^B \bar{\theta}_{ij}^t \bar{\theta}_{ij}^{t+1} - \left(\sum_{i=1}^B D_{i1j} \bar{\theta}_{i1j}^t \right) \left(\sum_{i_2=1}^B D_{i_2j} \bar{\theta}_{i_2j}^{t+1} \right) \right) \\
&= \frac{1}{n} \sum_{j=1}^n \left(n \sum_{i=1}^B \bar{\theta}_{ij}^t \bar{\theta}_{ij}^{t+1} - U_j V_j \right), \tag{59}
\end{aligned}$$

where, for $j = 1, \dots, n$, random variables U_j and V_j are defined as

$$U_j \triangleq \sqrt{n} \sum_{i=1}^B D_{ij} \bar{\theta}_{ij}^t,$$

and

$$V_j \triangleq \sqrt{n} \sum_{i=1}^B D_{ij} \bar{\theta}_{ij}^{t+1},$$

respectively.

Thus, Eq. (58), *i.e.*, the first two terms of (57), becomes,

$$\begin{aligned}
& 2 \sum_{i=1}^B \langle \tilde{\mathbf{x}}_i - \mathbf{x}_i^t, \tilde{\mathbf{x}}_i - \mathbf{x}_i^{t+1} \rangle \\
& - 2 \left\langle \sum_{i=1}^B \mathbf{D}_i (\tilde{\mathbf{x}}_i - \mathbf{x}_i^t), \sum_{i=1}^B \mathbf{D}_i (\tilde{\mathbf{x}}_i - \mathbf{x}_i^{t+1}) \right\rangle \\
&= 2 \|\boldsymbol{\theta}^t\|_2 \|\boldsymbol{\theta}^{t+1}\|_2 \frac{1}{n} \sum_{j=1}^n \left(n \sum_{i=1}^B \bar{\theta}_{ij}^t \bar{\theta}_{ij}^{t+1} - U_j V_j \right). \tag{60}
\end{aligned}$$

Impose the Cauchy-Schwarz inequality on the third term in (57), *i.e.*,

$$\begin{aligned}
& \left\langle \sum_{i=1}^B \mathbf{D}_i (\mathbf{x}_i - \tilde{\mathbf{x}}_i), \sum_{i=1}^B \mathbf{D}_i (\tilde{\mathbf{x}}_i - \mathbf{x}_i^{t+1}) \right\rangle \\
& \leq \left\| \sum_{i=1}^B \mathbf{D}_i (\mathbf{x}_i - \tilde{\mathbf{x}}_i) \right\|_2 \left\| \sum_{i=1}^B \mathbf{D}_i (\tilde{\mathbf{x}}_i - \mathbf{x}_i^{t+1}) \right\|_2 \\
&= \left\| \sum_{i=1}^B \mathbf{D}_i (\mathbf{x}_i - \tilde{\mathbf{x}}_i) \right\|_2 \left\| \sum_{i=1}^B \mathbf{D}_i \boldsymbol{\theta}_i^{t+1} \right\|_2. \tag{61}
\end{aligned}$$

Now, (57) becomes

$$\begin{aligned}
\sum_{i=1}^B \|\tilde{\mathbf{x}}_i - \mathbf{x}_i^{t+1}\|_2^2 & \leq 2 \|\boldsymbol{\theta}^t\|_2 \|\boldsymbol{\theta}^{t+1}\|_2 \frac{1}{n} \sum_{j=1}^n \left(n \sum_{i=1}^B \bar{\theta}_{ij}^t \bar{\theta}_{ij}^{t+1} - U_j V_j \right) \\
& + 2 \left\| \sum_{i=1}^B \mathbf{D}_i (\mathbf{x}_i - \tilde{\mathbf{x}}_i) \right\|_2 \left\| \sum_{i=1}^B \mathbf{D}_i \boldsymbol{\theta}_i^{t+1} \right\|_2, \tag{62}
\end{aligned}$$

which is

$$\begin{aligned} \|\boldsymbol{\theta}^{t+1}\|_2^2 &\leq 2\|\boldsymbol{\theta}^t\|_2\|\boldsymbol{\theta}^{t+1}\|_2\frac{1}{n}\sum_{j=1}^n\left(n\sum_{i=1}^B\bar{\theta}_{ij}^t\bar{\theta}_{ij}^{t+1}-U_jV_j\right) \\ &\quad + 2\left\|\sum_{i=1}^B\mathbf{D}_i(\mathbf{x}_i-\tilde{\mathbf{x}}_i)\right\|_2\left\|\sum_{i=1}^B\mathbf{D}_i\boldsymbol{\theta}_i^{t+1}\right\|_2. \end{aligned} \quad (63)$$

Dividing both sides by $\|\boldsymbol{\theta}^{t+1}\|_2$,

$$\begin{aligned} \|\boldsymbol{\theta}^{t+1}\|_2 &\leq 2\|\boldsymbol{\theta}^t\|_2\frac{1}{n}\sum_{j=1}^n\left(n\sum_{i=1}^B\bar{\theta}_{ij}^t\bar{\theta}_{ij}^{t+1}-U_jV_j\right) \\ &\quad + 2\left\|\sum_{i=1}^B\mathbf{D}_i(\mathbf{x}_i-\tilde{\mathbf{x}}_i)\right\|_2\left\|\sum_{i=1}^B\mathbf{D}_i\bar{\boldsymbol{\theta}}_i^{t+1}\right\|_2. \end{aligned} \quad (64)$$

In the following, we first bound the first term in (64) using the Theorem 5.

- Bounds using Bernstein type inequality.

Note that (U_j, V_j) , $j = 1, \dots, n$, are i.i.d. jointly Gaussian, such that

$$\begin{aligned} U_j &\sim \mathcal{N}\left(0, n\sum_{i=1}^B(\bar{\theta}_{ij}^t)^2\right), \\ V_j &\sim \mathcal{N}\left(0, n\sum_{i=1}^B(\bar{\theta}_{ij}^{t+1})^2\right) \end{aligned}$$

and

$$\mathbb{E}[U_jV_j] = n\sum_{i=1}^B\bar{\theta}_{ij}^t\bar{\theta}_{ij}^{t+1}.$$

By Lemma 1, since U_j and V_j are Gaussian random variables, U_jV_j is a sub-exponential random variable and

$$\|U_jV_j\|_{\psi_1} \leq \frac{8}{3}n\sqrt{\sum_{i=1}^B(\bar{\theta}_{ij}^t)^2\sum_{i=1}^B(\bar{\theta}_{ij}^{t+1})^2}. \quad (65)$$

On the other hand, $(\bar{\theta}_{ij}^t)^2$ and $(\bar{\theta}_{ij}^{t+1})^2$ are bounded as (52), i.e., $|\bar{\theta}_{ij}^t|^2 \leq \frac{\rho^2}{nB\delta}$, $|\bar{\theta}_{ij}^{t+1}|^2 \leq \frac{\rho^2}{nB\delta}$. Therefore,

$$\begin{aligned} \|U_jV_j\|_{\psi_1} &\leq \frac{8}{3}n\sum_{i=1}^B\frac{\rho^2}{nB\delta} \\ &= \frac{8\rho^2}{3\delta} \\ &\triangleq K. \end{aligned} \quad (66)$$

Define the set of possible normalized error vectors of interest as follows

$$\mathcal{F} \triangleq \left\{\frac{\mathbf{c}-\mathbf{c}'}{\|\mathbf{c}-\mathbf{c}'\|_2} : (\mathbf{c}, \mathbf{c}') \in \mathcal{C}^2, \|\mathbf{c}-\mathbf{c}'\|_2 \geq \sqrt{nB\delta}\right\}. \quad (67)$$

Employing Theorem 5 and (59), for a fixed $(\bar{\boldsymbol{\theta}}, \bar{\boldsymbol{\theta}}') \in \mathcal{F}^2$, we have

$$\begin{aligned}
& \Pr \left(\sum_{j=1}^n \left(\sum_{i=1}^B \bar{\theta}_{ij} \bar{\theta}'_{ij} - \left(\sum_{i=1}^B D_{ij} \bar{\theta}_{ij} \right) \left(\sum_{i=1}^B D_{ij} \bar{\theta}'_{ij} \right) \right) \geq \epsilon \right) \\
&= \Pr \left(\frac{1}{n} \sum_{j=1}^n \left(n \sum_{i=1}^B \bar{\theta}_{ij} \bar{\theta}_{ij} - U_j V_j \right) \geq \epsilon \right) \\
&\leq \exp \left\{ - \min \left(\frac{n\epsilon^2}{4K^2}, \frac{n\epsilon}{2K} \right) \right\} \\
&= \exp \left\{ - \left(\frac{n\epsilon}{2K} \right) \min \left(\frac{\epsilon}{2K}, 1 \right) \right\}, \tag{68}
\end{aligned}$$

where K is defined in (66) as $K \triangleq \frac{8\rho^2}{3\delta}$, and we have set $\{w_j\}_{j=1}^n = \frac{1}{n}$ in Theorem 5, and thus $\|\mathbf{w}\|_2^2 = \|\mathbf{w}\|_\infty = 1/n$. This leads to the final results in (68).

- Derive the union bound.

Given $\lambda > 0$, define event \mathcal{E}_1 as follows

$$\begin{aligned}
\mathcal{E}_1 &\triangleq \left\{ \sum_{j=1}^n \left(\sum_{i=1}^B \bar{\theta}_{ij} \bar{\theta}'_{ij} - \left(\sum_{i=1}^B D_{ij} \bar{\theta}_{ij} \right) \left(\sum_{i=1}^B D_{ij} \bar{\theta}'_{ij} \right) \right) \right. \\
&\quad \left. \leq \lambda : \forall (\bar{\boldsymbol{\theta}}, \bar{\boldsymbol{\theta}}') \in \mathcal{F}^2 \right\}. \tag{69}
\end{aligned}$$

Note the $\bar{\theta}_{ij} \bar{\theta}'_{ij}$ in (69) is different and $\bar{\theta}_{ij} \bar{\theta}'_{ij}$ in (68), where the one in (69) can be any value in a set \mathcal{F} , but the one in (68) is a fixed value.

Let $\{\mathcal{E}_i^c\}_{i=1}^3$ denote the complementary event of \mathcal{E}_i , and we need to consider all values in the set \mathcal{F} . Combining the union bound with (68) yields

$$\begin{aligned}
\Pr(\mathcal{E}_1^c) &\leq |\mathcal{F}|^2 \exp \left\{ - \left(\frac{n\lambda}{2K} \right) \min \left(\frac{\lambda}{2K}, 1 \right) \right\} \\
&\leq 2^{4nBr} \exp \left\{ - \left(\frac{n\lambda}{2K} \right) \min \left(\frac{\lambda}{2K}, 1 \right) \right\}, \tag{70}
\end{aligned}$$

where the second step follows because $|\mathcal{F}| \leq |\mathcal{C}|^2 \leq 2^{2nBr}$. Note that by assumption, $\delta \leq 16\rho^2/3$ and $0 < \lambda < 0.5$. Therefore,

$$\frac{\lambda}{2K} = \frac{3\lambda\delta}{16\rho^2} \leq \lambda < 1.$$

Therefore, (70) can be simplified as

$$\Pr(\mathcal{E}_1^c) \leq 2^{4nBr} \exp \left\{ - \left(\frac{3\delta}{16\rho^2} \right)^2 \lambda^2 n \right\}. \tag{71}$$

Conditioned on \mathcal{E}_1 , Eq. (64) becomes

$$\|\boldsymbol{\theta}^{t+1}\|_2 \leq 2\lambda\|\boldsymbol{\theta}^t\|_2 + 2\left\|\sum_{i=1}^B \mathbf{D}_i(\mathbf{x}_i - \tilde{\mathbf{x}}_i)\right\|_2 \left\|\sum_{i=1}^B \mathbf{D}_i \bar{\boldsymbol{\theta}}_i^{t+1}\right\|_2 \quad (72)$$

For fixed $\bar{\boldsymbol{\theta}} = \bar{\boldsymbol{\theta}}'$, (68) yields

$$\Pr\left(\left\|\sum_{i=1}^B \mathbf{D}_i \bar{\boldsymbol{\theta}}_i\right\|_2^2 \leq 1 - \epsilon\right) \leq \exp\left\{-\frac{n\epsilon^2}{4K^2}\right\}. \quad (73)$$

Using the same procedure, we can derive a counterpart to the above bound as follows

$$\Pr\left(\left\|\sum_{i=1}^B \mathbf{D}_i \bar{\boldsymbol{\theta}}_i\right\|_2^2 \geq 1 + \epsilon\right) \leq \exp\left\{-\frac{n\epsilon^2}{4K^2}\right\}. \quad (74)$$

Now we consider $\left\|\sum_{i=1}^B \mathbf{D}_i(\mathbf{x}_i - \tilde{\mathbf{x}}_i)\right\|_2$ and $\left\|\sum_{i=1}^B \mathbf{D}_i \bar{\boldsymbol{\theta}}_i^{t+1}\right\|_2$ in (72) separately.

a) Given $\epsilon_1 > 0$, define event \mathcal{E}_2 as

$$\mathcal{E}_2 \triangleq \left\{\frac{1}{n}\left\|\sum_{i=1}^B \mathbf{D}_i(\mathbf{x}_i - \tilde{\mathbf{x}}_i)\right\|_2^2 \leq \frac{1}{n}\|\mathbf{x} - \tilde{\mathbf{x}}\|_2^2 + B\rho^2\epsilon_1\right\}. \quad (75)$$

Note that by the definition of δ , we have

$$\|\mathbf{x} - \tilde{\mathbf{x}}\|_2^2 \leq nB\delta. \quad (76)$$

From (41), we have

$$\Pr(\mathcal{E}_2^c) \leq \exp\left\{-\min\left(\frac{n\epsilon_1^2}{4K'^2}, \frac{n\epsilon_1}{2K'}\right)\right\}, \quad (77)$$

where $K' = 8/3$.

Conditioned on \mathcal{E}_2 , we have

$$\begin{aligned} \left\|\sum_{i=1}^B \mathbf{D}_i(\mathbf{x}_i - \tilde{\mathbf{x}}_i)\right\|_2^2 &\leq \|\mathbf{x} - \tilde{\mathbf{x}}\|_2^2 + nB\rho^2\epsilon_1 \\ &\leq nB\delta + nB\rho^2\epsilon_1. \end{aligned} \quad (78)$$

This is

$$\left\|\sum_{i=1}^B \mathbf{D}_i(\mathbf{x}_i - \tilde{\mathbf{x}}_i)\right\|_2 \leq \sqrt{nB}\sqrt{\delta + \rho^2\epsilon_1}. \quad (79)$$

b) Given $\epsilon_2 > 0$, define event \mathcal{E}_3 as

$$\mathcal{E}_3 \triangleq \left\{\left\|\sum_{i=1}^B \mathbf{D}_i \bar{\boldsymbol{\theta}}_i\right\|_2^2 \leq 1 + \epsilon_2 : \forall \boldsymbol{\theta} \in \mathcal{F}\right\}. \quad (80)$$

Combining (74) with the union bound, we have

$$\begin{aligned} \Pr(\mathcal{E}_3^c) &\leq |\mathcal{F}| \exp\left\{-\frac{n\epsilon_2^2}{4K^2}\right\} \\ &\leq 2^{2nBr} \exp\left\{-\frac{n\epsilon_2^2}{4K^2}\right\}. \end{aligned} \quad (81)$$

Conditioned on $\mathcal{E}_1 \cap \mathcal{E}_2 \cap \mathcal{E}_3$, it follows from (72) that

$$\frac{1}{\sqrt{nB}} \|\boldsymbol{\theta}^{t+1}\|_2 \leq \frac{2\lambda}{\sqrt{nB}} \|\boldsymbol{\theta}^t\|_2 + 2\sqrt{(1+\epsilon_2)(\delta + \rho^2\epsilon_1)}. \quad (82)$$

Combining (71), (77) and (81), it follows that

$$\begin{aligned} \Pr(\mathcal{E}_1 \cap \mathcal{E}_2 \cap \mathcal{E}_3) &\geq 1 - \sum_{i=1}^3 \Pr(\mathcal{E}_i^c) \\ &\geq 1 - 2^{4nBr} \exp\left\{-\left(\frac{3\delta}{16\rho^2}\right)^2 \lambda^2 n\right\} \\ &\quad - \exp\left\{-\min\left(\frac{n\epsilon_1^2}{4K'^2}, \frac{n\epsilon_1}{2K'}\right)\right\} - 2^{2nBr} \exp\left\{-\frac{n\epsilon_2^2}{4K^2}\right\}. \end{aligned} \quad (83)$$

Now we set $\epsilon_1 = \delta/\rho^2$, $\epsilon_2 = 1$, we have

$$\begin{aligned} \min\left(\frac{n\epsilon_1^2}{4K'^2}, \frac{n\epsilon_1}{2K'}\right) &= \frac{n\epsilon_1}{2K'} \min\left(\frac{\epsilon_1}{2K'}, 1\right) \\ &\stackrel{K'=8/3}{=} \frac{3n\delta}{16\rho^2} \min\left(\frac{3\delta}{16\rho^2}, 1\right) \end{aligned} \quad (84)$$

$$\stackrel{\delta \leq 16\rho^2/3}{=} n \left(\frac{3\delta}{16\rho^2}\right)^2, \quad (85)$$

and

$$\frac{n\epsilon_2^2}{4K^2} \stackrel{K=8\rho^2/(3\delta)}{=} n \left(\frac{3\delta}{16\rho^2}\right)^2. \quad (86)$$

Therefore, (83) can be written as

$$\begin{aligned} \Pr(\mathcal{E}_1 \cap \mathcal{E}_2 \cap \mathcal{E}_3) &\geq 1 - 2^{4nBr} \exp\left\{-\left(\frac{3\delta}{16\rho^2}\right)^2 \lambda^2 n\right\} \\ &\quad - (2^{2nBr} + 1) \exp\left\{-n \left(\frac{3\delta}{16\rho^2}\right)^2\right\}. \end{aligned} \quad (87)$$

And (82) becomes

$$\frac{1}{\sqrt{nB}} \|\boldsymbol{\theta}^{t+1}\|_2 \leq \frac{2\lambda}{\sqrt{nB}} \|\boldsymbol{\theta}^t\|_2 + 4\sqrt{\delta}. \quad (88)$$

The main result will be

$$\frac{1}{\sqrt{nB}} \|\mathbf{x}^{t+1} - \tilde{\mathbf{x}}\|_2 \leq \frac{2\lambda}{\sqrt{nB}} \|\mathbf{x}^t - \tilde{\mathbf{x}}\|_2 + 4\sqrt{\delta}, \quad (89)$$

with probability at least

$$1 - 2^{4nBr} \exp \left\{ - \left(\frac{3\delta}{16\rho^2} \right)^2 \lambda^2 n \right\} - (2^{2nBr} + 1) \exp \left\{ -n \left(\frac{3\delta}{16\rho^2} \right)^2 \right\}. \quad (90)$$

□

C. Proof of Theorem 3

Proof. Define the error vector and the normalized error vector as (50) and (51), respectively. Using the same procedure as the one used in deriving (57), and noting that unlike in (57), here, the measurements are noisy and $\mathbf{y} = \sum_{i=1}^B \mathbf{D}_i \mathbf{x}_i + \mathbf{z}$, it follows that

$$\begin{aligned} \sum_{i=1}^B \|\boldsymbol{\theta}_i^{k+1}\|_2^2 &\leq 2 \sum_{i=1}^B \langle \boldsymbol{\theta}_i^{k+1}, \boldsymbol{\theta}_i^k \rangle - 2 \left\langle \sum_{i=1}^B \mathbf{D}_i \boldsymbol{\theta}_i^k, \sum_{i=1}^B \mathbf{D}_i \boldsymbol{\theta}_i^{k+1} \right\rangle \\ &\quad - 2 \left\langle \sum_{i=1}^B \mathbf{D}_i (\mathbf{x}_i - \tilde{\mathbf{x}}_i), \sum_{i=1}^B \mathbf{D}_i \boldsymbol{\theta}_i^{k+1} \right\rangle \\ &\quad + 2 \left| \sum_{i=1}^B \langle \mathbf{D}_i \mathbf{z}, \boldsymbol{\theta}_i^{k+1} \rangle \right|. \end{aligned} \quad (91)$$

Define the set of all possible normalized error vectors \mathcal{F} as in (67). Then, given $\lambda > 0$, $\epsilon_1 > 0$ and $\epsilon_2 > 0$, define events \mathcal{E}_1 , \mathcal{E}_2 and \mathcal{E}_3 as (69), (75) and (80), respectively. Conditioned on $\mathcal{E}_1 \cap \mathcal{E}_2 \cap \mathcal{E}_3$, using (82), (91) and setting ϵ_1 and ϵ_2 as before, it follows that

$$\|\boldsymbol{\theta}^{k+1}\|_2 \leq 2\lambda \|\boldsymbol{\theta}^k\|_2 + 4\sqrt{nB\delta} + 2 \left| \sum_{i=1}^B \langle \mathbf{D}_i \mathbf{z}, \bar{\boldsymbol{\theta}}_i^{k+1} \rangle \right|. \quad (92)$$

To finish the proof we need to bound $\left| \sum_{i=1}^B \langle \mathbf{D}_i \mathbf{z}, \bar{\boldsymbol{\theta}}_i^{k+1} \rangle \right|$. To achieve this goal, given $\epsilon_z \in (0, \sqrt{\rho})$, define event \mathcal{E}_z as follows,

$$\mathcal{E}_z \triangleq \left\{ \left| \sum_{i=1}^B \langle \mathbf{D}_i \mathbf{z}, \bar{\boldsymbol{\theta}}_i^{k+1} \rangle \right| \leq \sigma \sqrt{n} \epsilon_z : \forall \boldsymbol{\theta} \in \mathcal{F} \right\}. \quad (93)$$

Then, conditioned on $\mathcal{E}_1 \cap \mathcal{E}_2 \cap \mathcal{E}_3 \cap \mathcal{E}_z$, from (92), we have

$$\frac{1}{\sqrt{nB}} \|\boldsymbol{\theta}^{k+1}\|_2 \leq \frac{2\lambda}{\sqrt{nB}} \|\boldsymbol{\theta}^k\|_2 + 4\sqrt{\delta} + 2\epsilon_z \sigma, \quad (94)$$

which is the desired bound. The final step is to bound $\Pr(\mathcal{E}_z^c)$. Note that

$$\sum_{i=1}^B \langle \mathbf{D}_i \mathbf{z}, \bar{\boldsymbol{\theta}}_i^{k+1} \rangle = \left\langle \mathbf{z}, \sum_{i=1}^B \mathbf{D}_i \bar{\boldsymbol{\theta}}_i^{k+1} \right\rangle. \quad (95)$$

For fixed vector $\bar{\boldsymbol{\theta}}^{k+1}$, let $\boldsymbol{\kappa} = \sum_{i=1}^B \mathbf{D}_i \bar{\boldsymbol{\theta}}_i^{k+1}$. $\boldsymbol{\kappa}$ is a zero-mean Gaussian vector; let $\kappa_{i_1}, \kappa_{i_2}$ denote the i_1^{th} and i_2^{th} elements in $\boldsymbol{\kappa}$, respectively. We have

$$\begin{aligned} \mathbb{E} [\kappa_{i_1} \kappa_{i_2}] &= \mathbb{E} \left[\sum_{j_1=1}^B D_{j_1, (i_1, i_1)} \bar{\theta}_{j_1, i_1}^{k+1} \sum_{j_2=1}^B D_{j_2, (i_2, i_2)} \bar{\theta}_{j_2, i_2}^{k+1} \right] \\ &= \sum_{j_1=1}^B \sum_{j_2=1}^B \mathbb{E} [D_{j_1, (i_1, i_1)} D_{j_2, (i_2, i_2)}] \bar{\theta}_{j_1, i_1}^{k+1} \bar{\theta}_{j_2, i_2}^{k+1}, \end{aligned} \quad (96)$$

where $D_{j_1, (i_1, i_1)}$ denotes the $(i_1, i_1)^{th}$ element in matrix \mathbf{D}_i and $\bar{\theta}_{j_1, i_1}^{k+1}$ denotes the i_1^{th} element in the vector $\bar{\boldsymbol{\theta}}_{j_1}^{k+1}$, similar for $D_{j_2, (i_2, i_2)}$ and $\bar{\theta}_{j_2, i_2}^{k+1}$.

Since $\mathbb{E} [D_{j_1, (i_1, i_1)} D_{j_2, (i_2, i_2)}] = 0$, unless $j_1 = j_2$ and $i_1 = i_2$. Hence, for $i_1 \neq i_2$,

$$\mathbb{E} [\kappa_{i_1} \kappa_{i_2}] = 0.$$

For $i_1 = i_2 = i$, (96) simplifies to

$$\begin{aligned} \mathbb{E} [\kappa_i^2] &= \sum_{j_1=1}^B \sum_{j_2=1}^B \mathbb{E} [D_{j_1, (i, i)} D_{j_2, (i, i)}] \bar{\theta}_{j_1, i}^{k+1} \bar{\theta}_{j_2, i}^{k+1} \\ &= \sum_{j=1}^B \mathbb{E} [D_{j, (i, i)}^2] (\bar{\theta}_{j, i}^{k+1})^2 \\ &= \sum_{j=1}^B (\bar{\theta}_{j, i}^{k+1})^2. \end{aligned} \quad (97)$$

Therefore, in summary, for a fixed vector $\bar{\boldsymbol{\theta}}^{k+1}$, $\sum_{i=1}^B \mathbf{D}_i \bar{\boldsymbol{\theta}}_i^{k+1}$ is a zero-mean Gaussian vector in \mathbb{R}^n with independent entries. The variance of element i , κ_i , is characterized in (97). Therefore, $\kappa_i z_i$ are independent sub-exponential random variables. Moreover, as proved in the proof of Theorem 2, since by assumption $\|\boldsymbol{\theta}^k\|_2 \geq \sqrt{nB\delta}$ and $\|\boldsymbol{\theta}^{k+1}\|_2 \geq \sqrt{nB\delta}$, for $j = 1, \dots, B$ and $i = 1, \dots, n$, we have

$$|\bar{\theta}_{j, i}^{k+1}|^2 \leq \frac{\rho^2}{nB\delta}.$$

Hence,

$$\begin{aligned}
\|\kappa_i z_i\|_{\psi_1} &\leq \|\kappa_i\|_{\psi_2} \|z_i\|_{\psi_2} \\
&= \frac{8}{3} \sigma \left(\sum_{j=1}^B (\bar{\theta}_{j,i}^{k+1})^2 \right)^{\frac{1}{2}} \\
&\leq \frac{8\rho\sigma}{3\sqrt{n\delta}}.
\end{aligned} \tag{98}$$

Let $K = \frac{8}{3}$, using Theorem 5,

$$\begin{aligned}
\Pr \left(\sum_{i=1}^B \langle \mathbf{D}_i \mathbf{z}, \bar{\boldsymbol{\theta}}_i^{k+1} \rangle \geq \sigma \sqrt{n} \epsilon_z \right) &= \Pr \left(\sum_{i=1}^n \kappa_i z_i \geq \sigma \sqrt{n} \epsilon_z \right) \\
&\leq \exp \left\{ - \min \left(\frac{n \epsilon_z^2}{4 \frac{K^2 \rho^2}{n\delta} n}, \frac{\sqrt{n} \epsilon_z}{2 \frac{K\rho}{\sqrt{n\delta}}} \right) \right\} \\
&= \exp \left\{ - \left(\frac{n \epsilon_z \sqrt{\delta}}{2K\rho} \right) \min \left(\frac{\epsilon_z \sqrt{\delta}}{2K\rho}, 1 \right) \right\} \\
&= \exp \left\{ - \left(\frac{n \epsilon_z^2 \delta}{4K^2 \rho^2} \right) \right\} = \exp \left\{ -n \left(\frac{3\epsilon_z}{16\rho} \right)^2 \delta \right\},
\end{aligned} \tag{99}$$

where the last line follows since $\epsilon_z^2 \sqrt{\delta} < \rho$. Combining (99) with the union bound finishes the proof. \square

D. Proof of Theorem 4

Proof. Recall that $\mathbf{D}_i = \text{diag}(D_{i1}, \dots, D_{in})$, $\mathbf{H} = [\mathbf{D}_1, \dots, \mathbf{D}_B]$, and $\mathbf{R} = \mathbf{H}\mathbf{H}^\top = \text{diag}(R_1, \dots, R_n)$, where

$$R_j \triangleq \sum_{i=1}^B D_{ij}^2.$$

Using a derivation similar to (57) in Section V-B and noting that in GAP

$$\mathbf{s}_i^{t+1} = \mathbf{x}_i^t + B\mathbf{D}_i\mathbf{R}^{-1}\mathbf{e}^t,$$

it follows that

$$\begin{aligned}
& \sum_{i=1}^B \|\tilde{\mathbf{x}}_i - \mathbf{x}_i^{t+1}\|_2^2 \leq 2 \sum_{i=1}^B \langle \tilde{\mathbf{x}}_i - \mathbf{s}_i^{t+1}, \tilde{\mathbf{x}}_i - \mathbf{x}_i^{t+1} \rangle \\
& = 2 \sum_{i=1}^B \langle \tilde{\mathbf{x}}_i - \mathbf{x}_i^t - B\mathbf{D}_i\mathbf{R}^{-1}\mathbf{e}^t, \tilde{\mathbf{x}}_i - \mathbf{x}_i^{t+1} \rangle \\
& = 2 \sum_{i=1}^B \langle \tilde{\mathbf{x}}_i - \mathbf{x}_i^t, \tilde{\mathbf{x}}_i - \mathbf{x}_i^{t+1} \rangle \\
& \quad - 2B \sum_{i=1}^B \left\langle \mathbf{D}_i\mathbf{R}^{-1} \left(\mathbf{y} - \sum_{j=1}^B \mathbf{D}_j\mathbf{x}_j^t \right), \tilde{\mathbf{x}}_i - \mathbf{x}_i^{t+1} \right\rangle \\
& = 2 \sum_{i=1}^B \langle \tilde{\mathbf{x}}_i - \mathbf{x}_i^t, \tilde{\mathbf{x}}_i - \mathbf{x}_i^{t+1} \rangle \\
& \quad - 2B \sum_{i=1}^B \left\langle \sum_{j=1}^B \mathbf{D}_j(\mathbf{x}_j - \mathbf{x}_j^t), \mathbf{R}^{-1}\mathbf{D}_i(\tilde{\mathbf{x}}_i - \mathbf{x}_i^{t+1}) \right\rangle \\
& = 2 \sum_{i=1}^B \langle \tilde{\mathbf{x}}_i - \mathbf{x}_i^t, \tilde{\mathbf{x}}_i - \mathbf{x}_i^{t+1} \rangle \\
& \quad - 2B \left\langle \sum_{i=1}^B \mathbf{D}_i(\mathbf{x}_i - \tilde{\mathbf{x}}_i + \tilde{\mathbf{x}}_i - \mathbf{x}_i^t), \sum_{i=1}^B \mathbf{D}_i(\tilde{\mathbf{x}}_i - \mathbf{x}_i^{t+1}) \right\rangle \\
& = 2 \sum_{i=1}^B \langle \tilde{\mathbf{x}}_i - \mathbf{x}_i^t, \tilde{\mathbf{x}}_i - \mathbf{x}_i^{t+1} \rangle \\
& \quad - 2B \left\langle \sum_{i=1}^B \mathbf{D}_i(\tilde{\mathbf{x}}_i - \mathbf{x}_i^t), \mathbf{R}^{-1} \sum_{i=1}^B \mathbf{D}_i(\tilde{\mathbf{x}}_i - \mathbf{x}_i^{t+1}) \right\rangle \\
& \quad - 2B \left\langle \sum_{i=1}^B \mathbf{D}_i(\mathbf{x}_i - \tilde{\mathbf{x}}_i), \mathbf{R}^{-1} \sum_{i=1}^B \mathbf{D}_i(\tilde{\mathbf{x}}_i - \mathbf{x}_i^{t+1}) \right\rangle. \tag{100}
\end{aligned}$$

Defining $\boldsymbol{\theta}^t$ and $\bar{\boldsymbol{\theta}}^t$ as in (50) and (51), respectively, the first two terms in (100) can be written as

$$\begin{aligned}
& 2 \sum_{i=1}^B \langle \tilde{\mathbf{x}}_i - \mathbf{x}_i^t, \tilde{\mathbf{x}}_i - \mathbf{x}_i^{t+1} \rangle \\
& \quad - 2B \left\langle \sum_{i=1}^B \mathbf{D}_i(\tilde{\mathbf{x}}_i - \mathbf{x}_i^t), \mathbf{R}^{-1} \sum_{i=1}^B \mathbf{D}_i(\tilde{\mathbf{x}}_i - \mathbf{x}_i^{t+1}) \right\rangle \\
& = 2\|\boldsymbol{\theta}^t\|_2\|\boldsymbol{\theta}^{t+1}\|_2 \left(\sum_{i=1}^B \langle \bar{\boldsymbol{\theta}}_i^t, \bar{\boldsymbol{\theta}}_i^{t+1} \rangle \right. \\
& \quad \left. - B \left\langle \sum_{i=1}^B \mathbf{D}_i\bar{\boldsymbol{\theta}}_i^t, \mathbf{R}^{-1} \sum_{i=1}^B \mathbf{D}_i\bar{\boldsymbol{\theta}}_i^{t+1} \right\rangle \right). \tag{101}
\end{aligned}$$

Similarly, the third term in (100) can be written as

$$\begin{aligned} & \left\langle \sum_{i=1}^B \mathbf{D}_i (\mathbf{x}_i - \tilde{\mathbf{x}}_i), \mathbf{R}^{-1} \sum_{i=1}^B \mathbf{D}_i (\tilde{\mathbf{x}}_i - \mathbf{x}_i^{t+1}) \right\rangle \\ &= \|\boldsymbol{\theta}^{t+1}\|_2 \left\langle \sum_{i=1}^B \mathbf{D}_i (\mathbf{x}_i - \tilde{\mathbf{x}}_i), \mathbf{R}^{-1} \sum_{i=1}^B \mathbf{D}_i \bar{\boldsymbol{\theta}}_i^{t+1} \right\rangle. \end{aligned} \quad (102)$$

Hence, in summary, (100) can be written as

$$\begin{aligned} \|\boldsymbol{\theta}^{t+1}\|_2 &\leq 2B \left| \left\langle \sum_{i=1}^B \mathbf{D}_i (\mathbf{x}_i - \tilde{\mathbf{x}}_i), \mathbf{R}^{-1} \sum_{i=1}^B \mathbf{D}_i \bar{\boldsymbol{\theta}}_i^{t+1} \right\rangle \right| \\ &+ 2\|\boldsymbol{\theta}^t\|_2 \left(\sum_{i=1}^B \langle \bar{\boldsymbol{\theta}}_i^t, \bar{\boldsymbol{\theta}}_i^{t+1} \rangle - B \left\langle \sum_{i=1}^B \mathbf{D}_i \bar{\boldsymbol{\theta}}_i^t, \mathbf{R}^{-1} \sum_{i=1}^B \mathbf{D}_i \bar{\boldsymbol{\theta}}_i^{t+1} \right\rangle \right). \end{aligned} \quad (103)$$

Note that

$$\begin{aligned} & \sum_{i=1}^B \langle \bar{\boldsymbol{\theta}}_i^t, \bar{\boldsymbol{\theta}}_i^{t+1} \rangle - B \left\langle \sum_{i=1}^B \mathbf{D}_i \bar{\boldsymbol{\theta}}_i^t, \mathbf{R}^{-1} \sum_{i=1}^B \mathbf{D}_i \bar{\boldsymbol{\theta}}_i^{t+1} \right\rangle \\ &= \sum_{j=1}^n \left(\sum_{i=1}^B \bar{\theta}_{ij}^t \bar{\theta}_{ij}^{t+1} - \frac{B}{R_j} \left(\sum_{i_1=1}^B D_{i_1 j} \bar{\theta}_{i_1 j}^t \right) \left(\sum_{i_2=1}^B D_{i_2 j} \bar{\theta}_{i_2 j}^{t+1} \right) \right) \end{aligned} \quad (104)$$

For $j = 1, \dots, n$, define random variable P_j as follows

$$P_j \triangleq \frac{B}{R_j} \left(\sum_{i_1=1}^B D_{i_1 j} \bar{\theta}_{i_1 j}^t \right) \left(\sum_{i_2=1}^B D_{i_2 j} \bar{\theta}_{i_2 j}^{t+1} \right). \quad (105)$$

We first show that P_j is a bounded random variable. Applying the Cauchy-Schwarz inequality to both terms in P_j , we have

$$\begin{aligned} |P_j| &= \frac{B}{R_j} \left| \sum_{i_1=1}^B D_{i_1 j} \bar{\theta}_{i_1 j}^t \right| \left| \sum_{i_2=1}^B D_{i_2 j} \bar{\theta}_{i_2 j}^{t+1} \right| \\ &\leq \frac{B}{R_j} \sum_{i_1=1}^B D_{i_1 j}^2 \sqrt{\sum_{i_1=1}^B (\bar{\theta}_{i_1 j}^t)^2} \sqrt{\sum_{i_1=1}^B (\bar{\theta}_{i_1 j}^{t+1})^2} \\ &= B \sqrt{\sum_{i_1=1}^B (\bar{\theta}_{i_1 j}^t)^2 \sum_{i_1=1}^B (\bar{\theta}_{i_1 j}^{t+1})^2}. \end{aligned} \quad (106)$$

Next, we find the expected value of P_j . Note that

$$\begin{aligned} \mathbb{E}[P_j] &= \mathbb{E} \left[\frac{B}{R_j} \left(\sum_{i_1=1}^B D_{i_1 j} \bar{\theta}_{i_1 j}^t \right) \left(\sum_{i_2=1}^B D_{i_2 j} \bar{\theta}_{i_2 j}^{t+1} \right) \right] \\ &= B \sum_{i_1=1}^B \sum_{i_2=1}^B \mathbb{E} \left[\frac{D_{i_1 j} D_{i_2 j}}{R_j} \right] \bar{\theta}_{i_1 j}^t \bar{\theta}_{i_2 j}^{t+1}. \end{aligned} \quad (107)$$

But,

$$\sum_{i=1}^B \mathbb{E} \left[\frac{D_{ij}^2}{R_j} \right] = \mathbb{E} \left[\frac{\sum_{i=1}^B D_{ij}^2}{R_j} \right] = \frac{R_j}{R_j} = 1. \quad (108)$$

Moreover, by symmetry of the distributions,

$$\mathbb{E} \left[\frac{D_{1j}^2}{R_j} \right] = \dots = \mathbb{E} \left[\frac{D_{Bj}^2}{R_j} \right]. \quad (109)$$

Combing (108) and (109), it follows that

$$\mathbb{E} \left[\frac{D_{1j}^2}{R_j} \right] = \dots = \mathbb{E} \left[\frac{D_{Bj}^2}{R_j} \right] = \frac{1}{B}. \quad (110)$$

On the other hand, for $i_1 \neq i_2$, since D_{i_1j} and D_{i_2j} have symmetric distributions around zero, and are independent, we have

$$\mathbb{E} \left[\frac{D_{i_1j} D_{i_2j}}{R_j} \right] = 0. \quad (111)$$

Hence, inserting (110) and (111) in (107), we have

$$\begin{aligned} \mathbb{E}[P_j] &= \mathbb{E} \left[\frac{B}{R_j} \left(\sum_{i_1=1}^B D_{i_1j} \bar{\theta}_{i_1j}^t \right) \left(\sum_{i_2=1}^B D_{i_2j} \bar{\theta}_{i_2j}^{t+1} \right) \right] \\ &= \sum_{i=1}^B \bar{\theta}_{ij}^t \bar{\theta}_{ij}^{t+1}. \end{aligned} \quad (112)$$

These results show that (104) includes the sum of n independent bounded random variables. Therefore, using the Hoeffding's inequality, for fixed $\bar{\theta}^t$ and $\bar{\theta}^{t+1}$, for any $\lambda > 0$, we have

$$\begin{aligned} &\Pr \left(\sum_{j=1}^n \mathbb{E}[P_j] - \sum_{j=1}^n P_j \geq \lambda \right) \\ &\leq \exp \left\{ - \frac{2\lambda^2}{4B^2 \sum_{j=1}^n \sum_{i=1}^B (\bar{\theta}_{ij}^t)^2 \sum_{i=1}^B (\bar{\theta}_{ij}^{t+1})^2} \right\}. \end{aligned} \quad (113)$$

Note that by assumption

$$\frac{1}{nB} \sum_{i=1}^B \|\tilde{\mathbf{x}}_i - \mathbf{x}_i^t\|_2^2 \geq \delta.$$

Therefore, as argued before, for $i = 1, \dots, B$ and $j = 1, \dots, n$ in the proof of Theorem 2,

$$|\bar{\theta}_{ij}^t|^2 = \frac{(\tilde{x}_{ij} - x_{ij}^t)^2}{\|\boldsymbol{\theta}^t\|_2^2} \leq \frac{\rho^2}{nB\delta} \quad (114)$$

and, similarly,

$$|\bar{\theta}_{ij}^{t+1}|^2 \leq \frac{\rho^2}{nB\delta}. \quad (115)$$

Using the bounds in (115) and (115), it follows that

$$\begin{aligned} B^2 \sum_{j=1}^n \sum_{i=1}^B (\bar{\theta}_{ij}^t)^2 \sum_{i=1}^B (\bar{\theta}_{ij}^{t+1})^2 &\leq B^2 \sum_{j=1}^n \sum_{i=1}^B \left(\frac{\rho^2}{nB\delta} \right)^2 \\ &= B^2 nB \left(\frac{\rho^2}{nB\delta} \right)^2 = \frac{B\rho^4}{\delta^2 n}. \end{aligned} \quad (116)$$

Hence, from (113), for fixed $\bar{\theta}^t$ and $\bar{\theta}^{t+1}$, for any $\lambda > 0$, we have

$$\Pr \left(\sum_{j=1}^n \mathbb{E}[P_j] - \sum_{j=1}^n P_j \geq \lambda \right) \leq \exp \left\{ -\frac{\lambda^2 \delta^2 n}{2B\rho^4} \right\}. \quad (117)$$

Given $\lambda > 0$, define event \mathcal{E}_1 as follows

$$\mathcal{E}_1 \triangleq \left\{ \sum_{i=1}^B \langle \bar{\theta}_i^t, \bar{\theta}_i^{t+1} \rangle - B \left\langle \sum_{i=1}^B \mathbf{D}_i \bar{\theta}_i^t, \mathbf{R}^{-1} \sum_{i=1}^B \mathbf{D}_i \bar{\theta}_i^{t+1} \right\rangle \leq \lambda : \forall (\bar{\theta}, \bar{\theta}') \in \mathcal{F}^2 \right\}, \quad (118)$$

where the set of normalized error vectors \mathcal{F} is defined before in (67). Then, by the union bound, we have

$$\begin{aligned} \Pr(\mathcal{E}_1^c) &\leq |\mathcal{F}|^2 \exp \left\{ -\frac{\lambda^2 \delta^2 n}{2B\rho^4} \right\} \\ &\leq 2^{4nBr} \exp \left\{ -\frac{\lambda^2 \delta^2 n}{2B\rho^4} \right\}. \end{aligned} \quad (119)$$

We next bound the last term in (103). Note that

$$\begin{aligned} &\left\langle \sum_{i=1}^B \mathbf{D}_i (\mathbf{x}_i - \tilde{\mathbf{x}}_i), \mathbf{R}^{-1} \sum_{i=1}^B \mathbf{D}_i \bar{\theta}_i^{t+1} \right\rangle \\ &= \sum_{j=1}^n \frac{1}{R_j} \sum_{i=1}^B D_{ij} (x_{ij} - \tilde{x}_{ij}) \sum_{i=1}^B D_{ij} \bar{\theta}_{ij}^{t+1} \\ &= \sum_{j=1}^n \sum_{i_1=1}^B \sum_{i_2=1}^B \frac{D_{i_1 j} D_{i_2 j}}{R_j} (x_{i_1 j} - \tilde{x}_{i_1 j}) \bar{\theta}_{i_2 j}^{t+1}. \end{aligned} \quad (120)$$

For a fixed $\bar{\theta}^{t+1}$, and $j = 1, \dots, n$, define random variable Q_j as

$$Q_j = \sum_{i_1=1}^B \sum_{i_2=1}^B \frac{D_{i_1 j} D_{i_2 j}}{R_j} (x_{i_1 j} - \tilde{x}_{i_1 j}) \bar{\theta}_{i_2 j}^{t+1}. \quad (121)$$

Note that

$$\begin{aligned} \mathbb{E}[Q_j] &= \sum_{i_1=1}^B \sum_{i_2=1}^B \mathbb{E} \left[\frac{D_{i_1 j} D_{i_2 j}}{R_j} \right] (x_{i_1 j} - \tilde{x}_{i_1 j}) \bar{\theta}_{i_2 j}^{t+1} \\ &= \frac{1}{B} \sum_{i=1}^B (x_{ij} - \tilde{x}_{ij}) \bar{\theta}_{ij}^{t+1}. \end{aligned} \quad (122)$$

where the last line follows from (110) and (111). Therefore,

$$\begin{aligned}\sum_{j=1}^n \mathbb{E}[Q_j] &= \frac{1}{B} \sum_{j=1}^n \sum_{i=1}^B (x_{ij} - \tilde{x}_{ij}) \bar{\theta}_{ij}^{t+1} \\ &= \frac{1}{B} \langle \mathbf{x} - \tilde{\mathbf{x}}, \bar{\boldsymbol{\theta}}^{t+1} \rangle.\end{aligned}\quad (123)$$

Hence, by the Cauchy-Schwartz inequality,

$$\begin{aligned}\left| \sum_{j=1}^n \mathbb{E}[Q_j] \right| &\leq \frac{1}{B} \|\mathbf{x} - \tilde{\mathbf{x}}\|_2 \|\bar{\boldsymbol{\theta}}^{t+1}\|_2 \\ &\stackrel{\|\bar{\boldsymbol{\theta}}^{t+1}\|_2=1}{\leq} \frac{\sqrt{nB\delta}}{B} = \sqrt{\frac{n\delta}{B}}.\end{aligned}\quad (124)$$

Moreover, applying the Cauchy-Schwartz inequality twice, it follows that

$$\begin{aligned}|Q_j| &= \left| \sum_{i_1=1}^B \sum_{i_2=1}^B \frac{D_{i_1 j} D_{i_2 j}}{R_j} (x_{i_1 j} - \tilde{x}_{i_1 j}) \bar{\theta}_{i_2 j}^{t+1} \right| \\ &\leq \frac{\sum_{i=1}^B D_{i,j}^2}{R_j} \sqrt{\sum_{i=1}^B (x_{ij} - \tilde{x}_{ij})^2 \sum_{i=1}^B (\bar{\theta}_{ij}^{t+1})^2} \\ &= \sqrt{\sum_{i=1}^B (x_{ij} - \tilde{x}_{ij})^2 \sum_{i=1}^B (\bar{\theta}_{ij}^{t+1})^2}.\end{aligned}\quad (125)$$

Hence, Q_j , $j = 1, \dots, n$, are bounded independent random variables. Therefore, by the Hoeffding's inequality, it follows that, for any $\lambda' > 0$,

$$\begin{aligned}\Pr \left\{ \left\langle \sum_{i=1}^B \mathbf{D}_i (\mathbf{x}_i - \tilde{\mathbf{x}}_i), \mathbf{R}^{-1} \sum_{i=1}^B \mathbf{D}_i \bar{\boldsymbol{\theta}}_i^{t+1} \right\rangle - \sum_{j=1}^n \frac{1}{B} \sum_{i=1}^B (x_{ij} - \tilde{x}_{ij}) \bar{\theta}_{ij}^{t+1} \geq \lambda' \right\} \\ \leq \exp \left\{ -\frac{2\lambda'^2}{4 \sum_{j=1}^n \sum_{i=1}^B (x_{ij} - \tilde{x}_{ij})^2 \sum_{i=1}^B (\bar{\theta}_{ij}^{t+1})^2} \right\}\end{aligned}\quad (126)$$

But, from (115), it follows that

$$\begin{aligned}\sum_{j=1}^n \sum_{i=1}^B (x_{ij} - \tilde{x}_{ij})^2 \sum_{i=1}^B (\bar{\theta}_{ij}^{t+1})^2 &\leq \sum_{j=1}^n \sum_{i=1}^B (x_{ij} - \tilde{x}_{ij})^2 \sum_{i=1}^B \frac{\rho^2}{nB\delta} \\ &= \frac{\rho^2}{n\delta} \|\mathbf{x} - \tilde{\mathbf{x}}\|_2^2 \leq \rho^2 B.\end{aligned}\quad (127)$$

Letting

$$\lambda' = \sqrt{\frac{n\delta}{B}},$$

we have from (126) that

$$\begin{aligned} & \Pr \left\{ \left\langle \sum_{i=1}^B \mathbf{D}_i (\mathbf{x}_i - \tilde{\mathbf{x}}_i), \mathbf{R}^{-1} \sum_{i=1}^B \mathbf{D}_i \bar{\boldsymbol{\theta}}_i^{t+1} \right\rangle - \sum_{j=1}^n \frac{1}{B} \sum_{i=1}^B (x_{ij} - \tilde{x}_{ij}) \bar{\theta}_{ij}^{t+1} \geq \sqrt{\frac{n\delta}{B}} \right\} \\ & \leq \exp \left\{ -\frac{n\delta}{2\rho^2 B^2} \right\}. \end{aligned} \quad (128)$$

Define event \mathcal{E}_2 as

$$\mathcal{E}_2 = \left\{ \left\langle \sum_{i=1}^B \mathbf{D}_i (\mathbf{x}_i - \tilde{\mathbf{x}}_i), \mathbf{R}^{-1} \sum_{i=1}^B \mathbf{D}_i \bar{\boldsymbol{\theta}}_i^{t+1} \right\rangle \leq 2\sqrt{\frac{n\delta}{B}} : \forall \bar{\boldsymbol{\theta}} \in \mathcal{F} \right\}. \quad (129)$$

Then, using (128), (124) and the union bound, we have

$$\begin{aligned} \Pr(\mathcal{E}_2^c) & \leq |\mathcal{F}| \exp \left\{ -\frac{n\delta}{2\rho^2 B^2} \right\} \\ & \leq 2^{2nBr} \exp \left\{ -\frac{n\delta}{2\rho^2 B^2} \right\}. \end{aligned} \quad (130)$$

Finally, condition on $\mathcal{E}_1 \cap \mathcal{E}_2$, it follows from (101) that

$$\|\boldsymbol{\theta}^{t+1}\|_2 \leq 2\lambda \|\boldsymbol{\theta}^t\|_2 + 4B\sqrt{\frac{n\delta}{B}}, \quad (131)$$

or

$$\frac{1}{\sqrt{nB}} \|\mathbf{x}^{t+1} - \tilde{\mathbf{x}}\|_2 \leq \frac{2\lambda}{\sqrt{nB}} \|\mathbf{x}^t - \tilde{\mathbf{x}}\|_2 + 4\sqrt{\delta}, \quad (132)$$

which is the desired result. And the probability is

$$1 - 2^{2nBr} \exp \left\{ -\frac{n\delta}{2\rho^2 B^2} \right\} - 2^{4nBr} \exp \left\{ -\frac{\lambda^2 \delta^2 n}{2B\rho^4} \right\}. \quad (133)$$

□

VI. CONCLUSIONS

We have studied the problem of snapshot compressive sensing that rises in many modern compressive imaging applications. In such systems multiple signal frames are combined with each other, such that elements with the same (spatial, physical, etc.) locations are linearly combined together to form the measured signal frame. Therefore, the measured frame has the same dimensions of a single signal frame. A compression-based framework has been developed to theoretically analyze the snapshot compressive sensing systems. We have proposed two efficient recovery algorithms that reconstruct a high dimensional signal from its snapshot measurements. The proposed algorithms are compression-based recovery schemes that are theoretically proved to converge to the desired solution. Our simulation results for video snapshot CS show that the proposed methods achieve state-of-the art performance.

The proposed algorithms can be utilized in various snapshot compressive sensing applications, including videos, hyperspectral images, 3D scene compressive imaging [53], [54] and so on, thus filled the gap between existing compressive sensing theories and practical applications. We expect our proposed compression-based framework to be applied to and to inspire compressed sensing systems that capture ultrafast [5] and ultrahigh dimensional [20], [55], [56] data, and thus enable more advanced exploration of information in the nature.

APPENDIX A

DETAILS OF GAP-NLS

One drawback of the JPEG-based MPEG compression is that, since it relies on discrete Cosine transformation (DCT) of individual local patches, it does not exploit *nonlocal* similarities. In this section, we detail the proposed GAP-NLS algorithm. More specifically, we describe the encoder and decoder of the proposed compression code (NLS) that exploits nonlocal structures in videos. Figure 4 depicts our proposed NLS encoder/decoder.

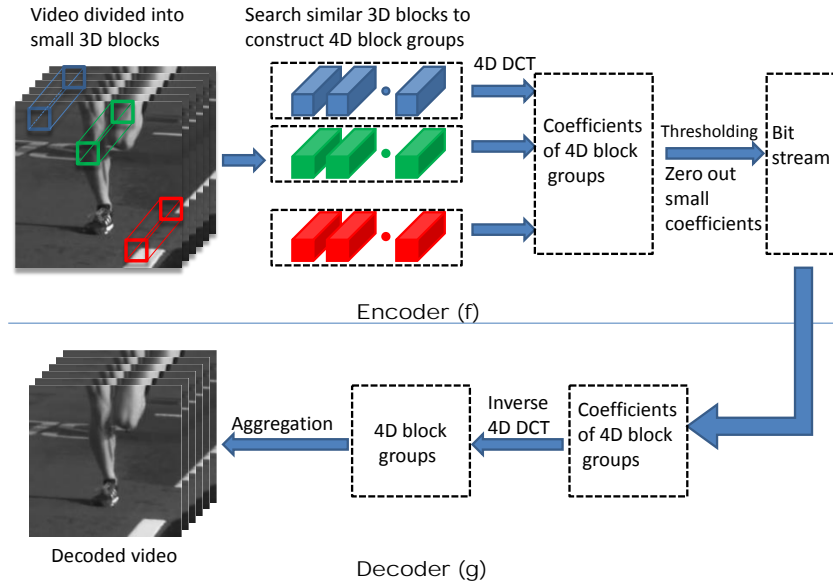


Fig. 4. Encoder (upper part) and decoder (lower part) by exploiting the nonlocal similarity of videos.

The encoding operation includes performing the following steps:

- i) Divide the 3D video $\mathbf{X} \in \mathbb{R}^{n_x \times n_y \times B}$ into small overlapping blocks $\mathcal{X}_q \in \mathbb{R}^{p_x \times p_y \times B}$, $q = 1, \dots, Q$, where Q denotes the number of such small 3D blocks.
- ii) For each *reference* block, \mathcal{X}_q , find its “similar” blocks between the remaining $Q - 1$ blocks. The similarity between two blocks is measured in terms of their ℓ_2 -norm distance. For \mathcal{X}_q , the encoder picks its G most similar blocks, thus forms a 4D tensor $\tilde{\mathcal{X}}_q \in \mathbb{R}^{p_x \times p_y \times B \times G}$.

- iii) Apply 4D DCT (discrete Cosine transformation) to each 4D block group, and derive the 4D coefficients for each block group. For each group of blocks, since the blocks are similar very, the coefficients will be sparse in the transform domain.
- iv) Set the coefficients with small amplitudes to zero. More specifically, the encoder only keeps $p_x p_y B$ (out of $p_x p_y bG$) coefficients with largest amplitudes for each block group. In total, there will be $p_x p_y BQ$ non-zero coefficients for the entire video since there are Q 3D blocks.
- v) Encode the remaining $p_x p_y BQ$ non-zero coefficients and their corresponding locations and their group indices.

Note that there are significant redundancies in this encoder since each pixel has been encoded many times, which will help the decoder to achieve videos with higher quality.

Correspondingly, the decoder includes the following steps.

- i) Decode the non-zero coefficients and their corresponding locations and group indices.
- ii) Fill in the zero coefficients to get the coefficients of 4D block groups.
- iii) Perform inverse 4D DCT to the coefficients of each 4D block group.
- iv) Put the blocks back to the original locations and aggregate these blocks (taking average value of each pixel) to achieve the decoded video.

REFERENCES

- [1] S. Jalali and X. Yuan, "Compressive imaging via one-shot measurements," in *Proc. IEEE Int. Symp. Inform. Theory*, 2018, pp. 416–420.
- [2] E. Candès, J. Romberg, , and T. Tao, "Robust uncertainty principles: Exact signal reconstruction from highly incomplete frequency information," *IEEE Trans. Inform. Theory*, vol. 52, no. 2, pp. 489–509, Feb. 2006.
- [3] D. L. Donoho, "Compressed sensing," *IEEE Trans. Inform. Theory*, vol. 52, no. 4, pp. 1289–1306, April 2006.
- [4] M. F. Duarte, M. A. Davenport, D. Takhar, J. N. Laska, T. Sun, K. F. Kelly, and R. G. Baraniuk, "Single-pixel imaging via compressive sampling," *IEEE Sig. Proc. Mag.*, vol. 25, no. 2, pp. 83–91, 2008.
- [5] L. Gao, J. Liang, C. Li, and L. V. Wang, "Single-shot compressed ultrafast photography at one hundred billion frames per second," *Nature*, vol. 516, pp. 49–57, 2014.
- [6] M. E. Gehm, R. John, D. J. Brady, R. M. Willett, and T. J. Schulz, "Single-shot compressive spectral imaging with a dual-disperser architecture," *Optics Exp.*, vol. 15, pp. 14 013–14 027, 2007.
- [7] Y. Hitomi, J. Gu, M. Gupta, T. Mitsunaga, and S. K. Nayar, "Video from a single coded exposure photograph using a learned over-complete dictionary," in *IEEE Int. Conf. on Comp. Vis. (ICCV)*, 2011.
- [8] P. Llull, X. Liao, X. Yuan, J. Yang, D. Kittle, L. Carin, G. Sapiro, and D. J. Brady, "Coded aperture compressive temporal imaging," *Optics Exp.*, vol. 21, no. 9, pp. 10 526–10 545, May 2013.
- [9] D. Reddy, A. Veeraraghavan, and R. Chellappa, "P2C2: Programmable pixel compressive camera for high speed imaging," *IEEE Comp. Vis. and Pat. Rec. (CVPR)*, 2011.
- [10] A. Wagadarikar, R. John, R. Willett, and D. J. Brady, "Single disperser design for coded aperture snapshot spectral imaging," *App. Optics*, vol. 47, no. 10, pp. B44–B51, 2008.
- [11] A. Wagadarikar, N. Pitsianis, X. Sun, and D. Brady, "Video rate spectral imaging using a coded aperture snapshot spectral imager," *Opt. Express*, vol. 17, no. 8, pp. 6368–6388, Apr. 2009.
- [12] G. Huang, H. Jiang, K. Matthews, and P. Wilford, "Lensless imaging by compressive sensing," *IEEE Int. Conf. on Image Proc.*, 2013.

- [13] A. C. Sankaranarayanan, L. Xu, C. Studer, Y. Li, K. F. Kelly, and R. G. Baraniuk, "Video compressive sensing for spatial multiplexing cameras using motion-flow models," *SIAM Journal on Imaging Sciences*, vol. 8, no. 3, pp. 1489–1518, 2015.
- [14] W. U. Bajwa, J. D. Haupt, G. M. Raz, S. J. Wright, and R. D. Nowak, "Toeplitz-structured compressed sensing matrices," in *2007 IEEE/SP 14th Workshop on Statistical Signal Processing*, Aug 2007, pp. 294–298.
- [15] A. Eftekhari, H. L. Yap, C. J. Rozell, and M. B. Wakin, "The restricted isometry property for random block diagonal matrices," *Appl. Comp. Harmonic Anal. (ACHA)*, vol. 38, no. 1, pp. 1 – 31, 2015.
- [16] J. Romberg, "Compressive sensing by random convolution," *SIAM Journal on Imaging Sciences*, vol. 2, no. 4, pp. 1098–1128, 2009.
- [17] P. Llull, X. Yuan, L. Carin, and D. Brady, "Image translation for single-shot focal tomography," *Optica*, vol. 2, no. 9, pp. 822–825, 2015.
- [18] X. Yuan, P. Llull, X. Liao, J. Yang, G. Sapiro, D. J. Brady, and L. Carin, "Low-cost compressive sensing for color video and depth," in *IEEE Conf. on Com. Vis. and Pat. Rec. (CVPR)*, 2014.
- [19] T.-H. Tsai, X. Yuan, and D. J. Brady, "Spatial light modulator based color polarization imaging," *Optics Express*, vol. 23, no. 9, pp. 11 912–11 926, May 2015.
- [20] T.-H. Tsai, P. Llull, X. Yuan, D. J. Brady, and L. Carin, "Spectral-temporal compressive imaging," *Optics Letters*, vol. 40, no. 17, pp. 4054–4057, Sep 2015.
- [21] E. Candes and J. Romberg, "Sparsity and incoherence in compressive sampling," *Inverse Problems*, vol. 23, no. 3, pp. 969–985, 2007.
- [22] I. Gorodnitsky and B. Rao, "Sparse signal reconstruction from limited data using focuss: A re-weighted minimum norm algorithm," *Trans. Sig. Proc.*, vol. 45, no. 3, pp. 600–616, Mar. 1997.
- [23] D. L. Donoho and M. Elad, "Optimally sparse representation in general (non-orthogonal) dictionaries via minimization," in *PROC. NATL ACAD. SCI. USA 100 2197202*, 2002.
- [24] R. M. Willett, R. F. Marcia, and J. M. Nichols, "Compressed sensing for practical optical imaging systems: a tutorial," *Optical Engineering*, vol. 50, 2011.
- [25] S. Jalali and A. Maleki, "From compression to compressed sensing," *Appl. Comp. Harmonic Anal. (ACHA)*, vol. 40, no. 2, pp. 352–385, 2016.
- [26] J. Yang, X. Yuan, X. Liao, P. Llull, G. Sapiro, D. J. Brady, and L. Carin, "Video compressive sensing using Gaussian mixture models," *IEEE Trans. on Image Proc.*, vol. 23, no. 11, pp. 4863–4878, Nov. 2014.
- [27] J. Yang, X. Liao, X. Yuan, P. Llull, D. J. Brady, G. Sapiro, and L. Carin, "Compressive sensing by learning a Gaussian mixture model from measurements," *IEEE Trans. on Image Proc.*, vol. 24, no. 1, pp. 106–119, Jan. 2015.
- [28] X. Yuan, T.-H. Tsai, R. Zhu, P. Llull, D. J. Brady, and L. Carin, "Compressive hyperspectral imaging with side information," *IEEE J. of Sel. Topics in Sig. Proc.*, vol. 9, no. 6, pp. 964–976, Sep. 2015.
- [29] J. Huang, T. Zhang, and D. Metaxas, "Learning with structured sparsity," *Ann. Int. Conf. on Mac. Learning (ICML)*, pp. 417–424, 2009.
- [30] R. G. Baraniuk, V. Cevher, M. F. Duarte, and C. Hegde, "Model-based compressive sensing," *IEEE Trans. Inform. Theory*, vol. 56, no. 4, pp. 1982–2001, April 2010.
- [31] W. Dong, G. Shi, X. Li, Y. Ma, and F. Huang, "Compressive sensing via nonlocal low-rank regularization," *EEE Trans. on Image Proc.*, vol. 23, no. 8, pp. 3618–3632, 2014.
- [32] C. A. Metzler, A. Maleki, and R. G. Baraniuk, "From denoising to compressed sensing," *IEEE Trans. Inform. Theory*, vol. 62, no. 9, pp. 5117–5144, Sep. 2016.
- [33] D. S. Taubman and M. W. Marcellin, *JPEG2000: Image Compression Fundamentals, Standards and Practice*. Kluwer Academic Publishers, 2002.
- [34] S. Beygi, S. Jalali, A. Maleki, and U. Mitra, "An efficient algorithm for compression-based compressed sensing," *To appear in Information and Inference: A Journal of IMA*, 2018.
- [35] J. Holloway, A. C. Sankaranarayanan, A. Veeraraghavan, and S. Tambe, "Flutter shutter video camera for compressive sensing of videos," in *2012 IEEE International Conference on Computational Photography (ICCP)*, April 2012, pp. 1–9.
- [36] H. Arguello, H. Rueda, Y. Wu, D. W. Prather, and G. R. Arce, "Higher-order computational model for coded aperture spectral imaging," *Appl. Opt.*, vol. 52, no. 10, pp. D12–D21, Apr 2013.

- [37] R. G. Baraniuk, T. Goldstein, A. C. Sankaranarayanan, C. Studer, A. Veeraraghavan, and M. B. Wakin, “Compressive video sensing: Algorithms, architectures and applications,” *IEEE Signal Processing Magazine*, vol. 34, no. 1, pp. 52–66, Jan 2017.
- [38] G. R. Arce, D. J. Brady, L. Carin, H. Arguello, and D. S. Kittle, “Compressive coded aperture spectral imaging: An introduction,” *IEEE Signal Processing Magazine*, vol. 31, no. 1, pp. 105–115, Jan 2014.
- [39] X. Cao, T. Yue, X. Lin, S. Lin, X. Yuan, Q. Dai, L. Carin, and D. J. Brady, “Computational snapshot multispectral cameras: Toward dynamic capture of the spectral world,” *IEEE Signal Processing Magazine*, vol. 33, no. 5, pp. 95–108, Sept 2016.
- [40] X. Liao, H. Li, and L. Carin, “Generalized alternating projection for weighted- $\ell_{2,1}$ minimization with applications to model-based compressive sensing,” *SIAM Journal on Imaging Sciences*, vol. 7, no. 2, pp. 797–823, 2014.
- [41] M. Iliadis, L. Spinoulas, and A. K. Katsaggelos, “Deep fully-connected networks for video compressive sensing,” *Digital Signal Processing*, vol. 72, pp. 9 – 18, 2018.
- [42] K. Xu and F. Ren, “CSVideoNet: A real-time end-to-end learning framework for high-frame-rate video compressive sensing,” *ArXiv e-prints*, Dec. 2016.
- [43] X. Yuan, “Generalized alternating projection based total variation minimization for compressive sensing,” in *IEEE Int. Conf. on Image Proc. (ICIP)*, Sep. 2016, pp. 2539–2543.
- [44] D. Le Gall, “MPEG: A video compression standard for multimedia applications,” *Communications of the ACM*, vol. 34, no. 4, pp. 46–58, Apr. 1991.
- [45] J. A. Nelder and R. Mead, “A simplex method for function minimization,” *Computer Journal*, vol. 7, pp. 308–313, 1965.
- [46] A. Buades, B. Coll, and J.-M. Morel, “A non-local algorithm for image denoising,” in *IEEE Conf. on Comp. Vis. and Pat. Rec. (CVPR’05)*, 2005, pp. 60–5.
- [47] K. Dabov, A. Foi, V. Katkovnik, and K. Egiazarian, “Image denoising by sparse 3d transform-domain collaborative filtering,” *EEE Trans. on Image Proc.*, vol. 16, no. 8, pp. 2080–2095, August 2007.
- [48] M. Maggioni, G. Boracchi, A. Foi, and K. Egiazarian, “Video denoising, deblocking and enhancement through separable 4-d nonlocal spatiotemporal transforms,” *EEE Trans. on Image Proc.*, vol. 21, no. 9, pp. 3952–3966, Sept 2012.
- [49] W. Dong, L. Zhang, G. Shi, and X. Li, “Nonlocally centralized sparse representation for image restoration,” *EEE Trans. on Image Proc.*, vol. 22, no. 4, pp. 1620–1630, April 2013.
- [50] H. Liu, R. Xiong, J. Zhang, and W. Gao, “Image denoising via adaptive soft-thresholding based on non-local samples,” in *2015 IEEE Conf. on Com. Vis. and Pat. Rec. (CVPR)*, June 2015, pp. 484–492.
- [51] “Runner data,” <https://www.videvo.net/video/elite-runner-slow-motion/4541/>.
- [52] R. Vershynin, “Introduction to the non-asymptotic analysis of random matrices,” *arXiv preprint arXiv:1011.3027*, 2010.
- [53] Y. Sun, X. Yuan, and S. Pang, “High-speed compressive range imaging based on active illumination,” *Optics Express*, vol. 24, no. 20, pp. 22 836–22 846, Oct 2016.
- [54] —, “Compressive high-speed stereo imaging,” *Optics Express*, vol. 25, no. 15, pp. 18 182–18 190, July 2017.
- [55] D. Huang, E. Swanson, C. Lin, J. Schuman, W. Stinson, W. Chang, M. Hee, T. Flotte, K. Gregory, C. Puliafito, and a. et, “Optical coherence tomography,” *Science*, vol. 254, no. 5035, pp. 1178–1181, 1991.
- [56] A. Kirmani, D. Venkatraman, D. Shin, A. Colaço, F. N. C. Wong, J. H. Shapiro, and V. K. Goyal, “First-photon imaging,” *Science*, vol. 343, no. 6166, pp. 58–61, 2014.